Supplementary Information (SI) for Inorganic Chemistry Frontiers.

A Benzoxazolyl-Linked Cyclic(alkyl)(amino)carbene (CAAC): the *N*- Sidearm Negatively Influences the Buchwald-Hartwig Coupling

Soumajit Nath,[a] Subham Sarkar,[a,b] Sudip Baguli,[a] Ankit Kumar,[a] Dibyendu Mallick,[b,*] and Debabrata Mukherjee[a,*]

[a] Department of Chemical Sciences, Indian Institute of Science Education and Research Kolkata, West Bengal, 741246, India. Email: d.mukherjee@iiserkol.ac.in

[b] Department of Chemistry, Presidency University, 86/1 College Street, Kolkata, West Bengal, 700073, India. E-mail: dibyendu.chem@presiuniv.ac.in

Table of Contents

1. General Methods.

All the experiments were carried out under dry and oxygen-free nitrogen using standard Schlenk techniques or in an argon-filled glovebox (MBraun), unless otherwise stated. Prior to use, glassware was dried overnight at 130 °C and solvents were dried, distilled and degassed using standard methods and stored on activated 4 Å molecular sieves in the glovebox. **1**,[1] *N*-(2,6-diisopropylphenyl)benzimidoyl chloride,[2] and the enamine **EA**[3] were made from literature procedures. Anhydrous CuCl, AgCl, $Pd(COD)Cl_2$, and $AgSbF_6$ were purchased from Sigma-Aldrich and used as received in the glovebox. $(Bu_4N)Cl$ and $(Bu_4N)BF_4$ were purchased from Hyma and BLD, respectively, and used without further purification. The substrates were purchased from various suppliers like Hyma, Spectrochem, and BLD and used without further purification. The ^1H, $^{13}C\{^1H\}$, ^{11}B, and ^{19}F NMR spectra were recorded either on JEOL-ECZ (400 MHz) or on Bruker spectrometers (Avance NEO or Avance III) operating at 500 MHz at ambient temperature. Structural assignments were made with additional information from gCOSY, gHSQC, and gDEPT experiments. Mass spectrometric analyses were done on a Waters Spectrometer. X-ray diffraction data were collected either on a Rigaku Synergy i xtalab diffractometer or on a Bruker D8 diffractometer. Elemental analyses were performed on a PerkinElmer series II 2400 machine. All NMR spectra, a summary of crystal data and structural refinements, and a summary of computational details are given in their respective sections. The crystallographic data for the structures reported in this article have been deposited at the Cambridge Crystallographic Data Centre, under the deposition numbers CCDC- 2482323 (**2**), 2482324 (**3**), 2482325 (**4**), and 2482326 (**5**). The data can be obtained free of charge via https://www.ccdc.cam.ac.uk/structures/.

2. Synthetic Procedure and Spectroscopic Characterization.

2. A 50 mL Teflon-stoppered storage flask fitted with a magnetic bead was charged with **1** (0.200 g, 0.497 mmol), CuCl (0.108 g, 1.092 mmol), and 3 mL of THF. The mixture was then heated at 55 °C for 18 h under constant stirring to obtain a yellow suspension. The volatiles were removed from the reaction mixture under reduced pressure to obtain a yellow residue. The latter was extracted with CH_2Cl_2 and filtered. Volatiles were again removed from the filtrate to obtain a sticky brown solid. Washing it with excess of benzene and hexane, respectively, and drying under vacuum afforded **2** (0.347 g, 0.577 mmol, 86%) as a yellowish solid. X-ray quality single crystals were grown from a concentrated THF solution at room temperature.

^1H NMR (500 MHz, $CDCl_3$): δ 7.90 – 7.82 (m, 1H, Ar-*H*), 7.61 – 7.55 (m, 1H, Ar-*H*), 7.43 – 7.39 (m, 2H, Ar-*H*), 7.31 – 7.24 (m, 2H, Ar-*H*), 7.22 (d, *J* = 7.7 Hz, 1H, Ar-*H*), 3.87 (d, *J* = 15.3 Hz, 1H, Ar-C*H*H), 3.46 (d, *J* = 15.2 Hz, 1H, Ar-C*H*H), 2.83 (td, *J* = 13.1, 5.7 Hz, 2H, ^{i}Pr-C*H*, ring-CH_2), 2.69 (p, *J* = 6.8 Hz, 1H, ^{i}Pr-C*H*), 2.13 (d, *J* = 13.5 Hz, 1H, ring-CH_2), 1.67 (s, 3H, CH_3), 1.42 (s, 3H, CH_3), 1.37 – 1.28 (m, 9H, CH_3), 1.13 (d, *J* = 6.7 Hz, 3H, CH_3), 1.03 (d, *J* = 6.6 Hz, 3H, CH_3). $^{13}C\{^1H\}$ NMR (126 MHz, $CDCl_3$) δ 222.8, 145.5, 145.0, 129.9, 128.3, 125.4, 124.9, 124.7, 119.8, 110.8, 45.6, 39.1, 29.1, 28.9, 28.8, 27.7, 27.3, 27.2, 22.4, 22.1. Anal. Calc. for $C_{54}H_{68}Cl_4Cu_4N_4O_2$: C, 54.00; H, 5.71; N, 4.66. Found: C 53.78; H, 5.68; N, 4.74.

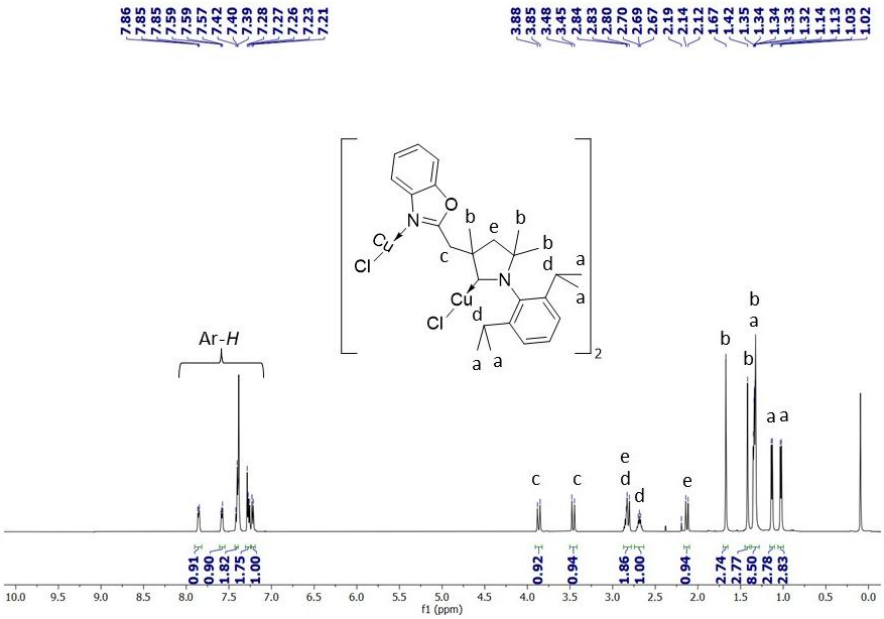

Figure S1. ^1H NMR spectrum (500 MHz) of **2** in $CDCl_3$.

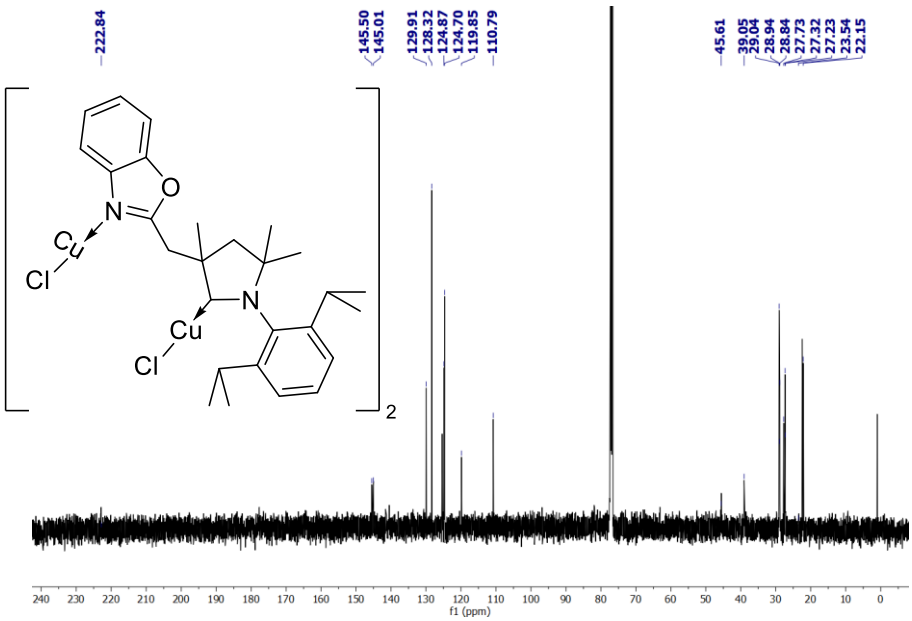

Figure S2. $^{13}C\{^{1}H\}$ NMR spectrum (126 MHz) of **2** in $CDCl_3$.

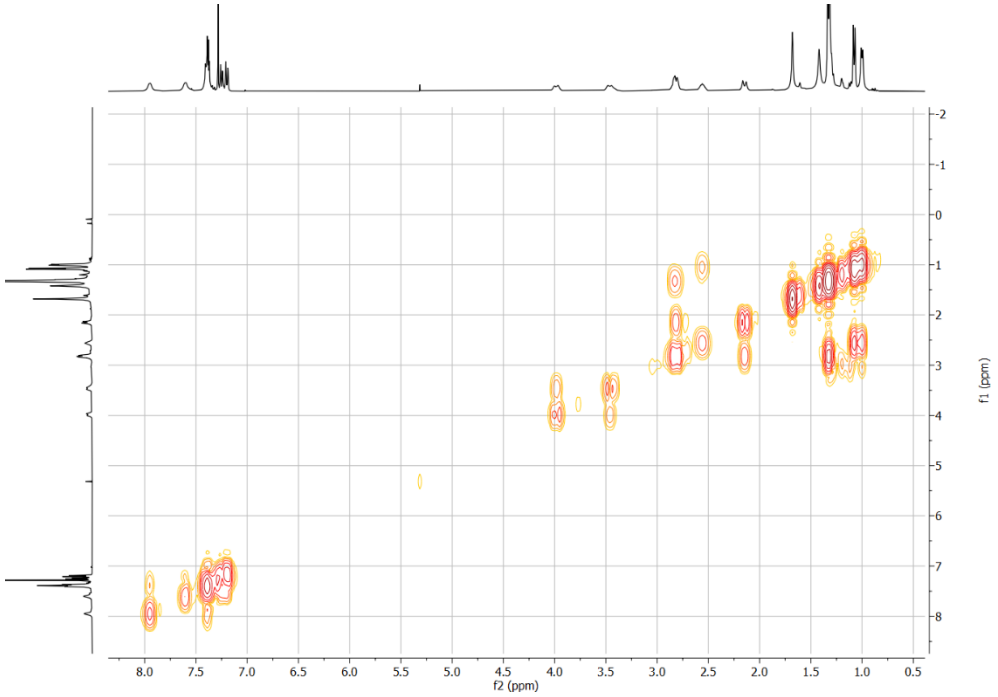

Figure S3. (^{1}H -^{1}H) COSY NMR spectrum (500 MHz) of **2** in $CDCl_3$.

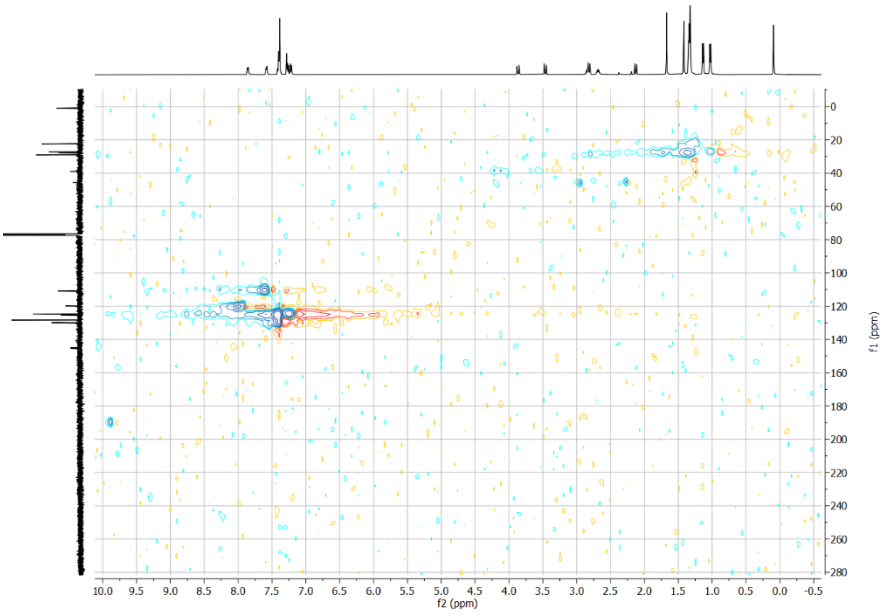

Figure S4. (^{1}H -^{13}C) HSQC NMR spectrum (500 MHz) of **2** in $CDCl_3$.

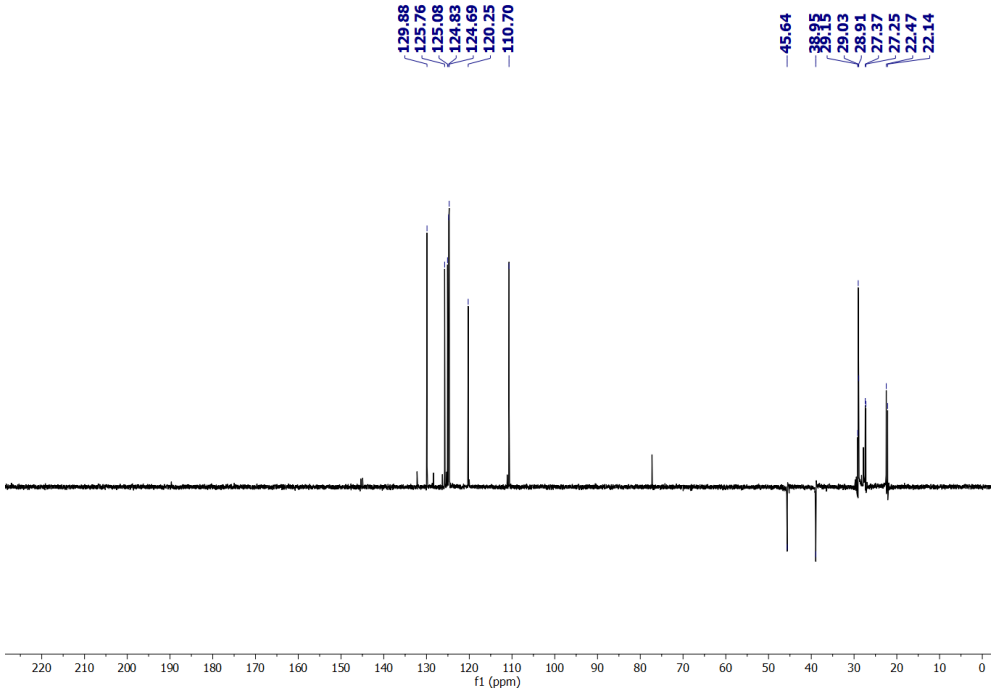

Figure S5. DEPT-^{13}C NMR spectrum (126 MHz) of **2** in $CDCl_3$.

3. A 50 mL Teflon-stoppered storage flask fitted with a magnetic stir bar was charged with **1** (0.200 g, 0.497 mmol), AgCl (0.078 g, 0.546 mmol), and 3 mL of THF. The mixture was then heated at 90 °C for 36 h under constant stirring to obtain a dark solution. It was filtered through a short pad of celite and the volatiles were removed from the filtrate under reduced pressure to obtain an off-white residue. Washing the latter with excess of benzene and hexane, respectively, and drying under vacuum gave **3** (0.343 g, 0.629 mmol, 79%) as an off-white solid. X-ray quality single crystals were grown from hexane diffusion into a THF solution at –35 °C.

^{1}H NMR (400 MHz, $CDCl_3$): δ 7.68 – 7.61 (m, 1H, Ar-*H*), 7.56 – 7.49 (m, 1H, Ar-*H*), 7.42 – 7.30 (m, 3H, Ar-*H*), 7.22 (dd, *J* = 9.2, 7.8, 1.5 Hz, 3H, Ar-*H*), 3.60 (d, *J* = 15.9 Hz, 1H, Ar-C*H*H), 3.33 (d, *J* = 15.9 Hz, 1H, Ar-CH*H*), 2.91 (p, *J* = 6.7 Hz, 1H, ^{i}Pr-C*H*), 2.84 – 2.75 (m, 2H, ^{i}Pr-C*H*, ring-CH_2), 2.08 (d, *J* = 13.3 Hz, 1H, ring-CH_2), 1.42 (s, 3H, CH_3), 1.34 (s, 3H, CH_3), 1.30 (dd, *J* = 6.8, 1.9 Hz, 6H, CH_3), 1.17 (d, *J* = 6.8 Hz, 3H, CH_3), 0.98 (d, *J* = 6.6 Hz, 3H, CH_3). ^{13}C{^{1}H} NMR (101 MHz, $CDCl_3$) δ 252.9 (dd, $J_{13C\text{-}109Ag}$ = 246.9 Hz, $J_{13C\text{-}107Ag}$ = 214.1 Hz), 163.3, 150.6, 145.7, 145.1, 141.1, 130.2, 125.3, 125.2, 125.0, 124.6, 119.6, 111.0, 83.9, 83.8, 57.9, 57.8, 44.7, 44.6, 38.8, 29.0, 28.7, 27.7, 27.5, 22.7, 22.4. Anal. Calc. for $C_{27}H_{34}AgClN_2O$: C, 59.41; H, 6.28; N, 5.13. Found: C 59.22; H, 6.32; N, 5.24.

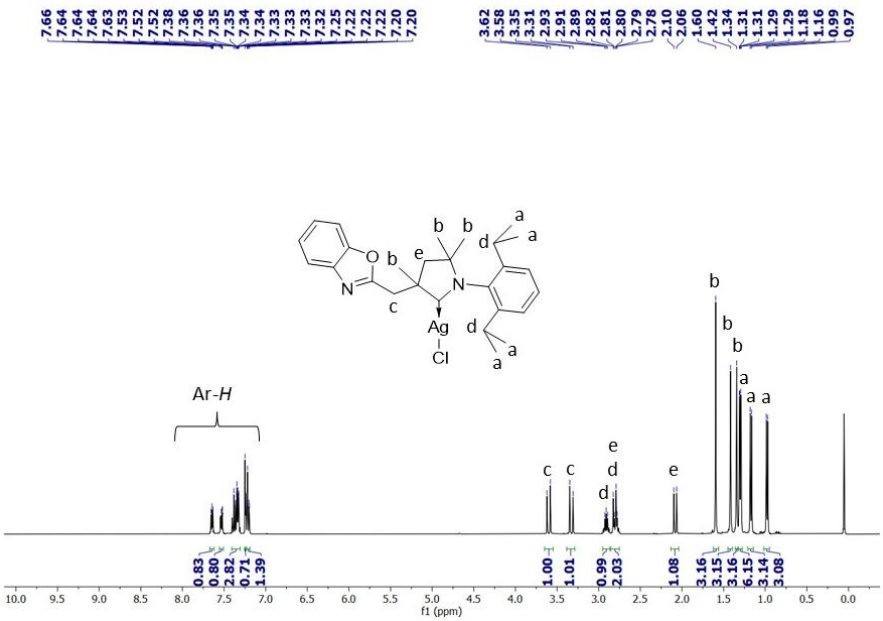

Figure S6. ^{1}H NMR spectrum (400 MHz) of **3** in $CDCl_3$.

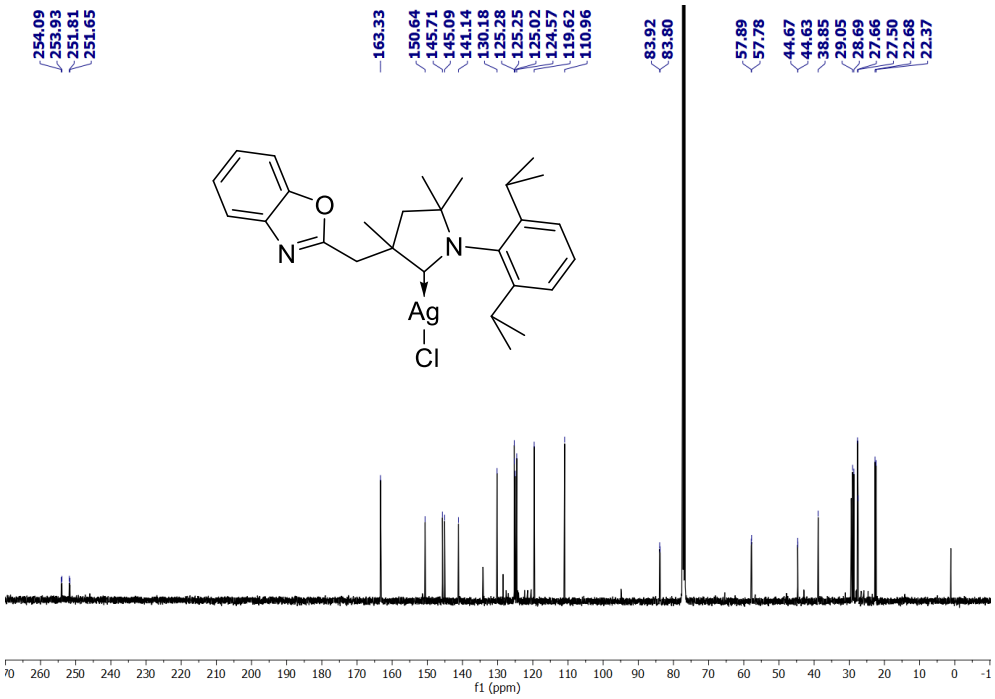

Figure S7. $^{13}C\{^{1}H\}$ NMR spectrum (101 MHz) of **3** in $CDCl_3$.

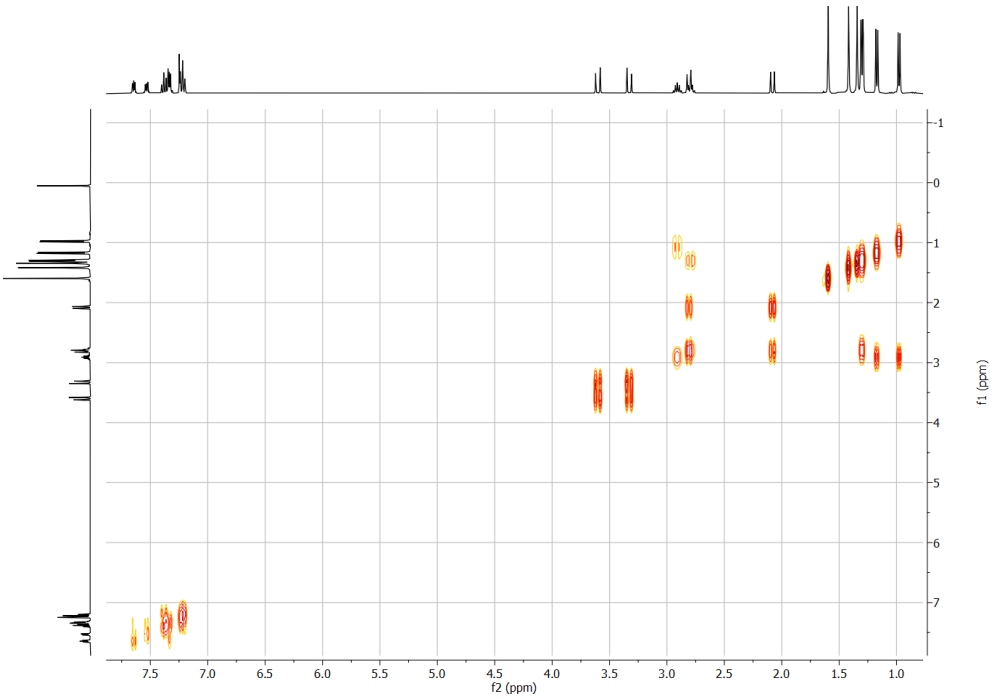

Figure S8. (^{1}H -^{1}H) COSY NMR spectrum (400 MHz) of **3** in $CDCl_3$.

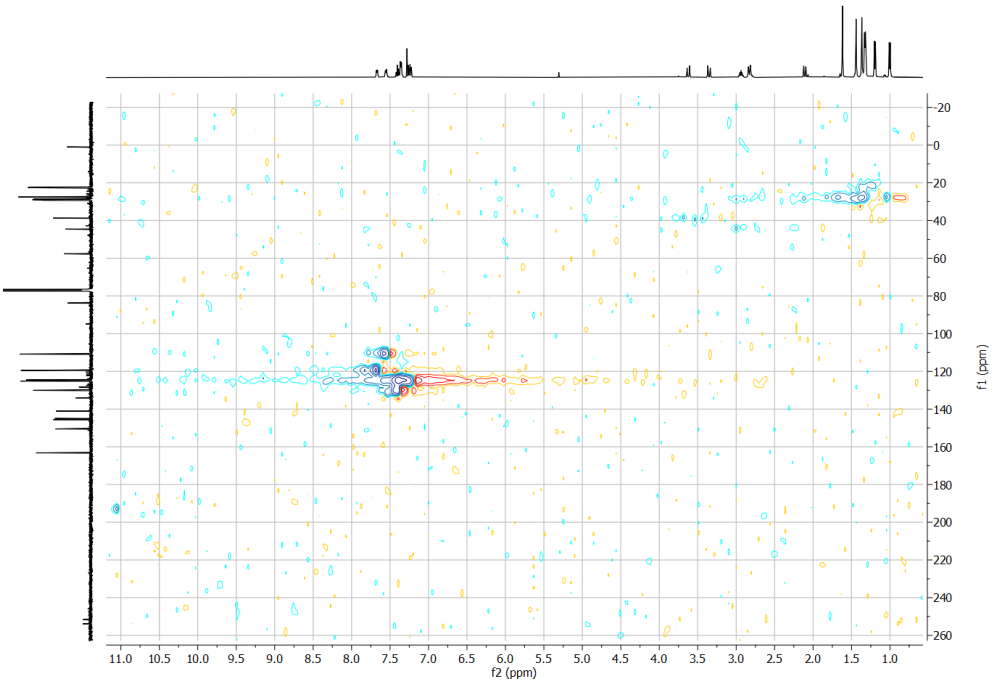

Figure S9. (^{1}H -^{13}C) HSQC NMR spectrum (400 MHz) of **3** in $CDCl_3$.

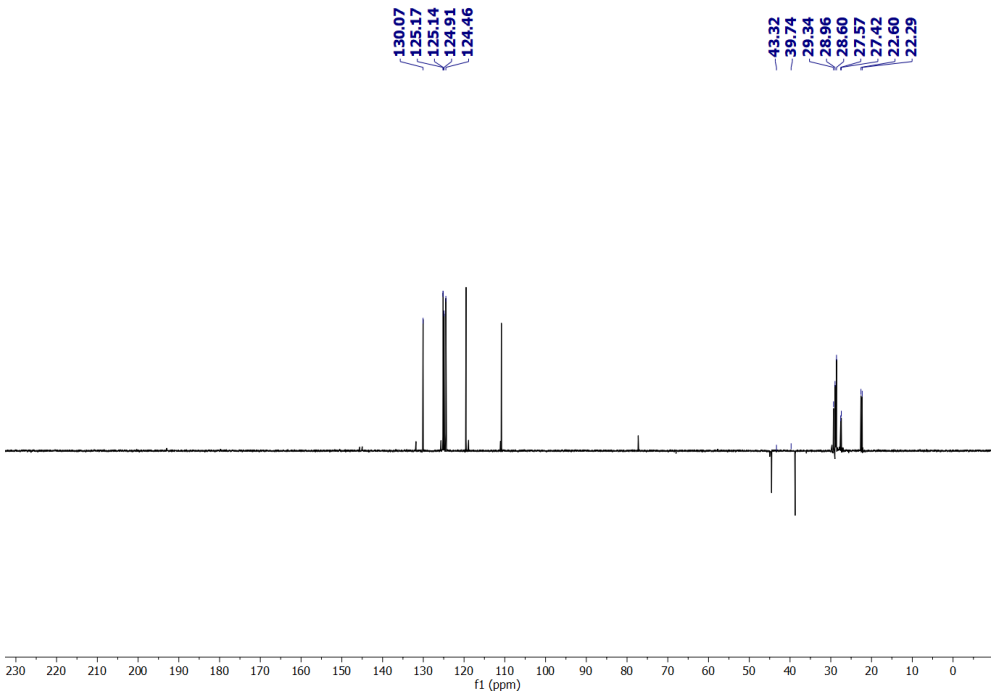

Figure S10. DEPT-^{13}C NMR spectrum (101 MHz) of **3** in $CDCl_3$.

4. A 50 mL Teflon-stoppered storage flask fitted with a magnetic bead was charged with **2** (0.200 g, 0.333 mmol), Pd(COD)Cl_2 (0.095 g, 0.333 mmol), and 4 mL CH_2Cl_2. The mixture was heated at 60 °C for 10 h under constant stirring to obtain a yellow solution with a grey precipitate. It was filtered through a short pad of celite and the volatiles were removed from the filtrate under reduced pressure to obtain a yellow residue. The latter was washed with excess of hexane and dried under vacuum to afford **4** (0.244 g, 0.421 mmol, 79%) as a bright yellow crystalline solid. X-ray quality single crystals were grown from hexane diffusion into a THF solution at –35 °C.

Alternatively, a 10 mL screw-cap vial fitted with a magnetic bead was charged with **3** (0.200 g, 0.366 mmol), Pd(COD)Cl_2 (0.104 g, 0.366 mmol), and 4 mL of CH_2Cl_2. The mixture was stirred at room temperature for 10 hours in dark to obtain a yellow solution with a grey precipitate. It was filtered through a short pad of celite and the volatiles were removed from the filtrate under reduced pressure to obtain a yellow residue. It was washed with excess of hexane and dried under vacuum to afford **4** (0.211 g, 0.387 mmol, 86%) as a bright yellow crystalline solid.

^{1}H NMR (500 MHz, $CDCl_3$): δ 8.30 (s, 1H, Ar-*H*), 7.58 (d, *J* = 8.5 Hz, 1H, Ar-*H*), 7.44 (t, *J* = 7.8 Hz, 2H, Ar-*H*), 7.34 (dd, *J* = 26.9, 8.6 Hz, 2H, Ar-*H*), 7.27 (s, 1H, Ar-*H*), 3.99 (s, 1H, Ar-CH*H*), 3.56 (d, *J* = 18.1 Hz, 1H, Ar-C*H*H), 2.79 (s, 1H, ^{i}Pr-C*H*), 2.36 (s, 3H, ^{i}Pr-C*H*, ring-CH_2), 2.16 (s, 3H, CH_3), 1.58 (d, *J* = 6.7 Hz, 3H, CH_3), 1.53 – 1.46 (m, 6H, CH_3), 1.32 (d, *J* = 6.5 Hz, 3H, CH_3), 1.14 (s, 3H, CH_3), 0.99 (d, *J* = 6.7 Hz, 3H, CH_3). ^{13}C{^{1}H}NMR (101 MHz, $CDCl_3$) δ 232.2, 150.1, 146.6, 145.1, 132.3, 130.0, 126.9, 126.3, 125.3, 125.2, 111.3, 83.5, 55.5, 53.5, 39.4, 29.9, 29.7, 29.7, 29.3, 26.4, 24.1. Anal. Calc. for $C_{27}H_{34}Cl_2N_2OPd$: C, 55.92; H, 5.91; N, 4.83. Found: C 55.56; H, 5.89; N, 4.88.

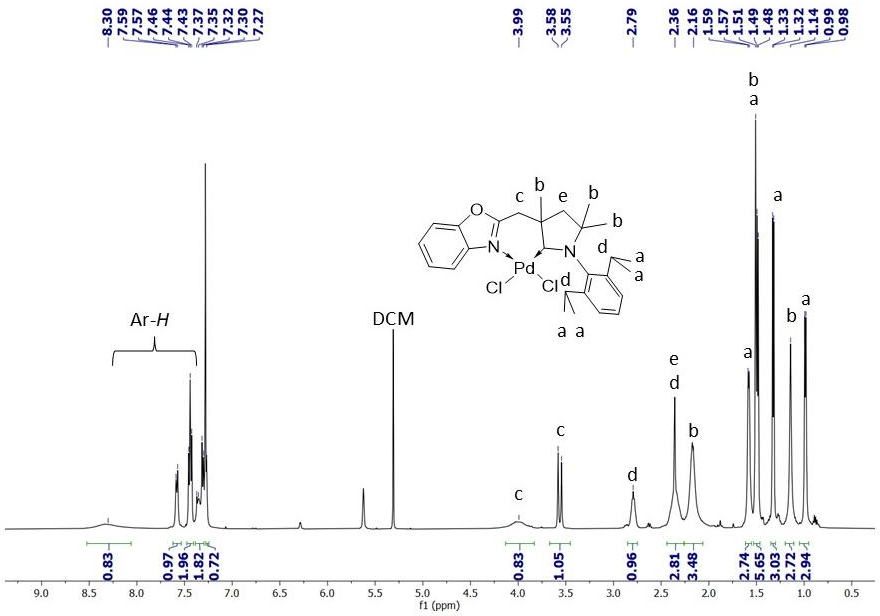

Figure S11. ^{1}H NMR spectrum (500 MHz) of **4** in $CDCl_3$.

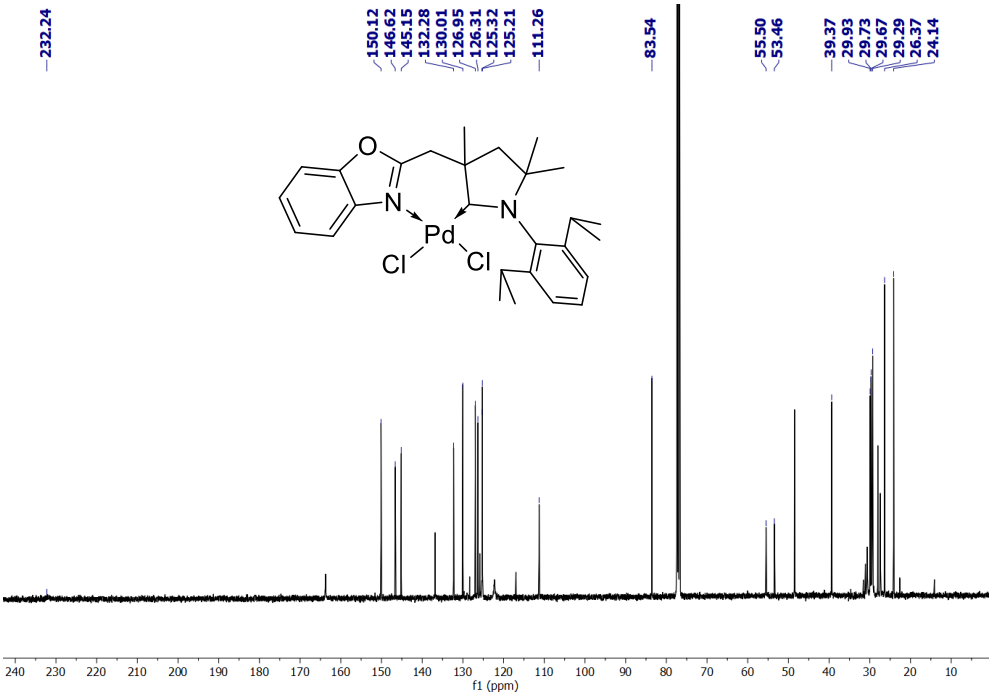

Figure S12. $^{13}C\{^{1}H\}$ NMR spectrum (101 MHz) of **4** in $CDCl_3$.

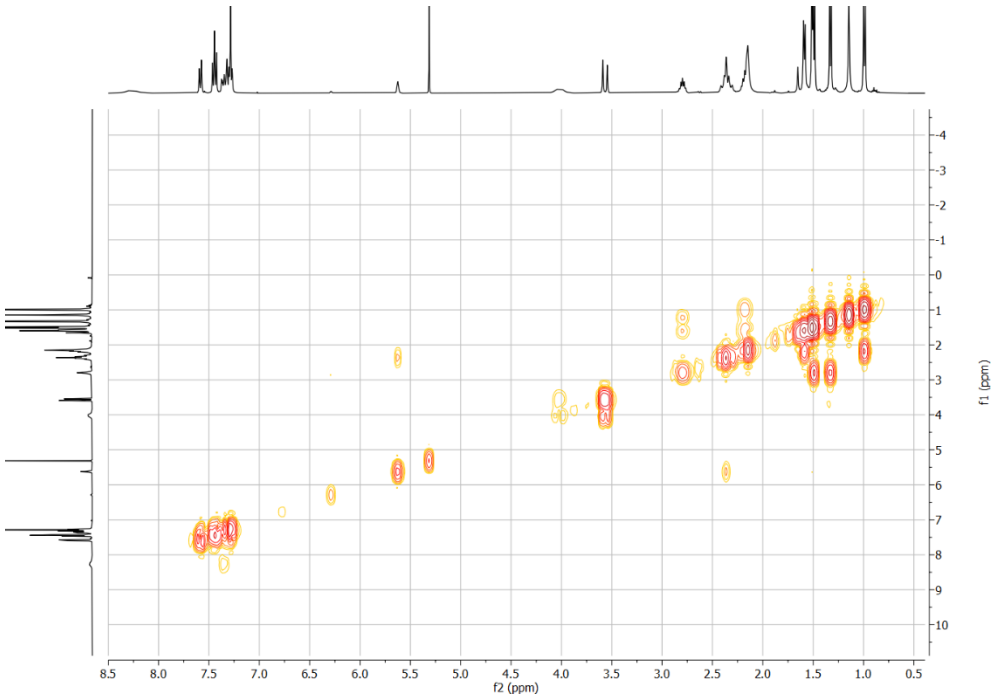

Figure S13. (^{1}H -^{1}H) COSY NMR spectrum (500 MHz) of **4** in $CDCl_3$.

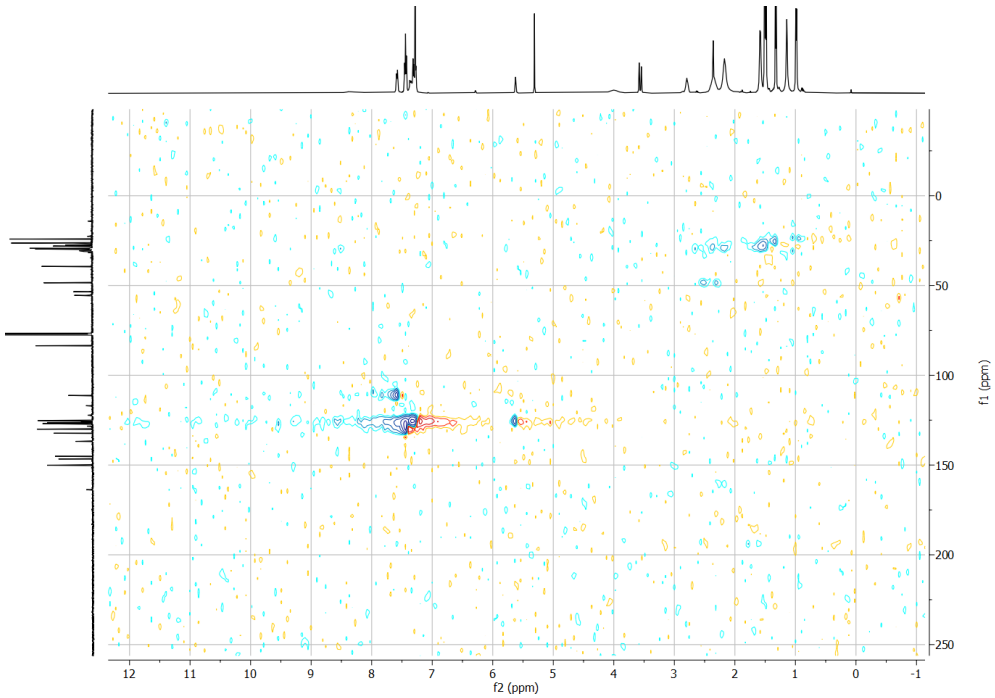

Figure S14. (^{1}H -^{13}C) HSQC NMR spectrum (500 MHz) of **4** in $CDCl_3$.

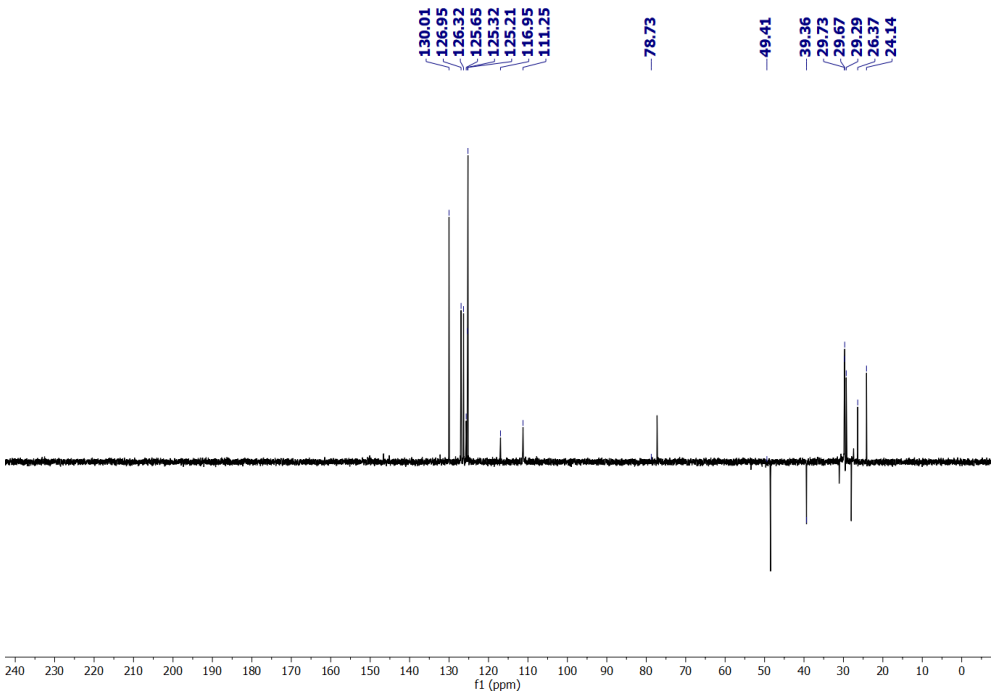

Figure S15. DEPT-^{13}C NMR spectrum (126 MHz) of **4** in $CDCl_3$.

5. A 10 mL screw-cap vial equipped with a magnetic stir bar was charged with **4** (0.200 g, 0.344 mmol), $AgSbF_6$ (0.118 g, 0.344 mmol), and 3 mL acetonitrile. The mixture was stirred at room temperature for 12 hours to obtain a yellow solution with a grey precipitate. It was filtered through a short pad of celite, and the volatiles were removed under reduced pressure to obtain a sticky residue. The latter was washed with excess of hexane and dried under vacuum to afford **5** (0.367 g, 0.471 mmol, 78%) as an off-white crystalline solid. X-ray quality single crystals were grown in concentrated acetonitrile solution at –35 °C.

^{1}H NMR (500 MHz, CD_3CN): δ 7.83 (d, *J* = 8.3 Hz, 1H, Ar-*H*), 7.78 (d, *J* = 8.4 Hz, 1H, Ar-*H*), 7.64 (dd, *J* = 25.9, 8.2 Hz, 4H, Ar-*H*), 7.52 (d, *J* = 7.4 Hz, 1H, Ar-*H*), 3.96 (d, *J* = 19.5 Hz, 1H, Ar-C*H*H), 3.70 (d, *J* = 19.5 Hz, 1H, Ar-CH*H*), 2.75 (dp, *J* = 26.0, 6.8 Hz, 2H, ^{i}Pr-C*H*), 2.54 (s, 2H, ring-CH_2), 2.06 (s, 3H, CH_3), 1.80 (d, *J* = 6.7 Hz, 3H, CH_3), 1.55 (s, 3H, CH_3), 1.43 (s, 3H, CH_3), 1.36 (d, *J* = 6.6 Hz, 3H, CH_3), 1.25 (d, *J* = 6.6 Hz, 3H, CH_3), 1.19 (d, *J* = 6.6 Hz, 3H, CH_3). ^{13}C{^{1}H} NMR (101 MHz, CD_3CN) δ 215.8, 165.7, 150.4, 145.6, 145.4, 136.0, 132.7, 131.7, 128.1, 126.9, 126.5, 125.9, 118.8, 112.3, 87.5, 54.2, 46.8, 37.1, 30.8, 29.2, 28.9, 28.8, 26.9, 26.7, 24.1, 24.1, 23.9. ^{19}F NMR (376 MHz, CD_3CN) δ -110.88, -113.96, -116.01, -121.16, -126.30, -131.45, -133.51, -136.59. Anal. Calc. for $C_{54}H_{68}Cl_2F_{12}N_4O_2Pd_2Sb_2$: C, 41.57; H, 4.39; N, 3.59. Found: C 41.38; H, 4.43; N, 3.64.

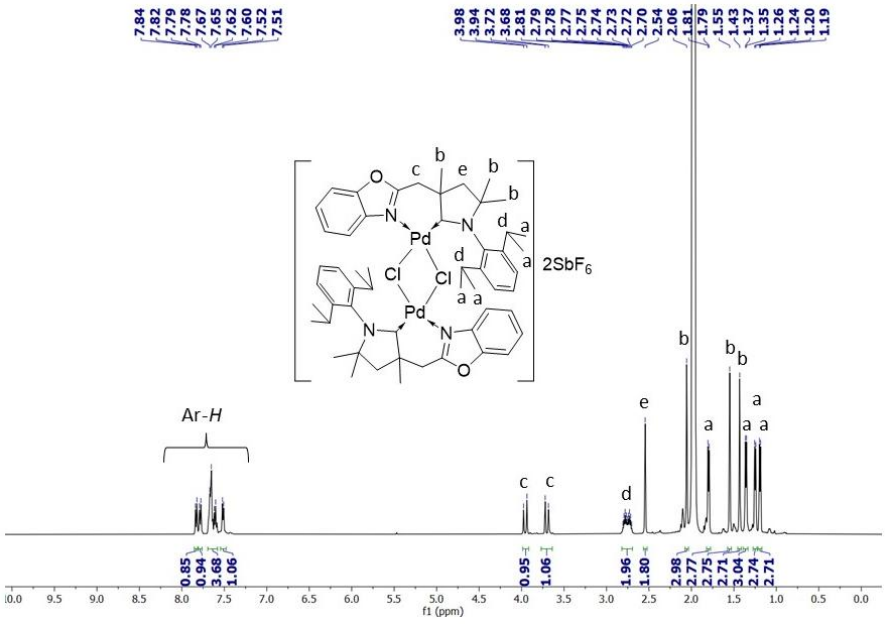

Figure S16. ^{1}H NMR spectrum (500MHz) of **5** in CD_3CN.

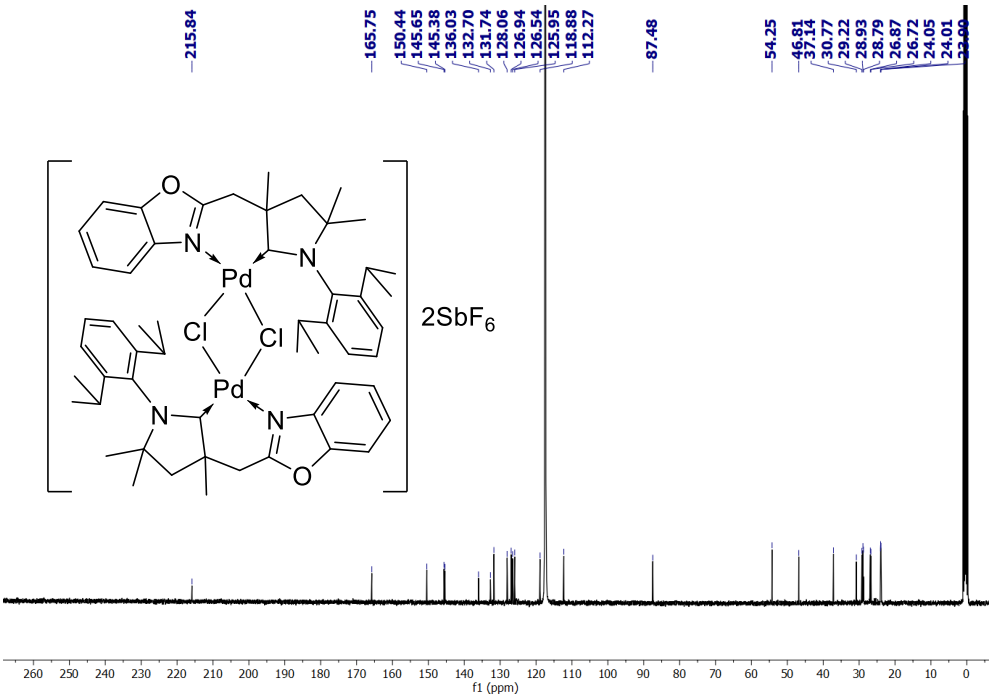

Figure S17. $^{13}C\{^{1}H\}$ NMR spectrum (101 MHz) of **5** in CD_3CN.

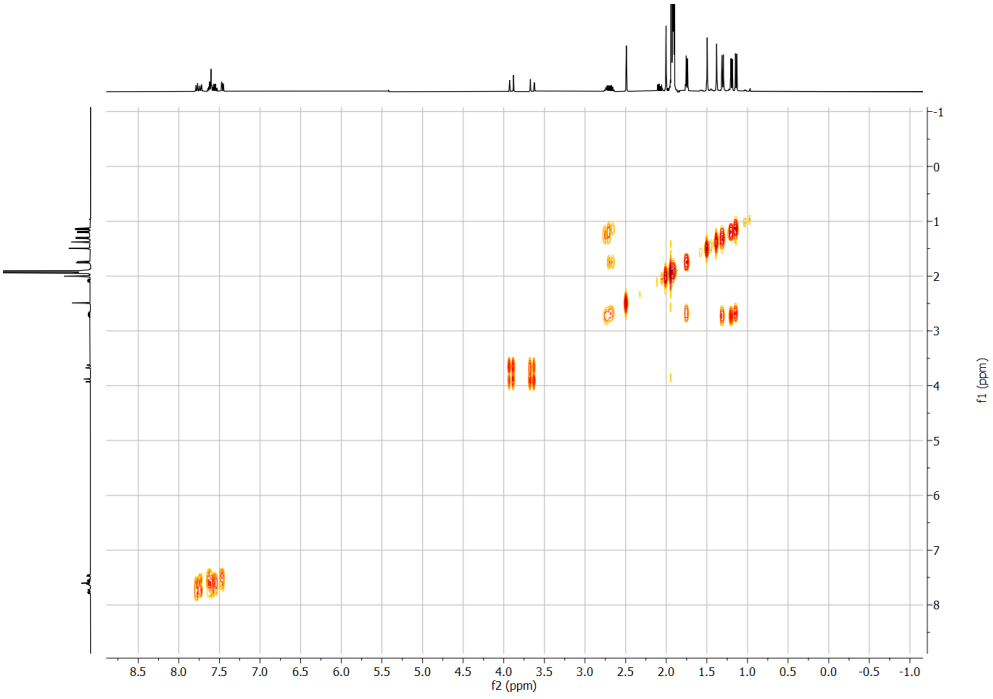

Figure S18. (^{1}H -^{1}H) COSY NMR spectrum (500MHz) of **5** in CD_3CN.

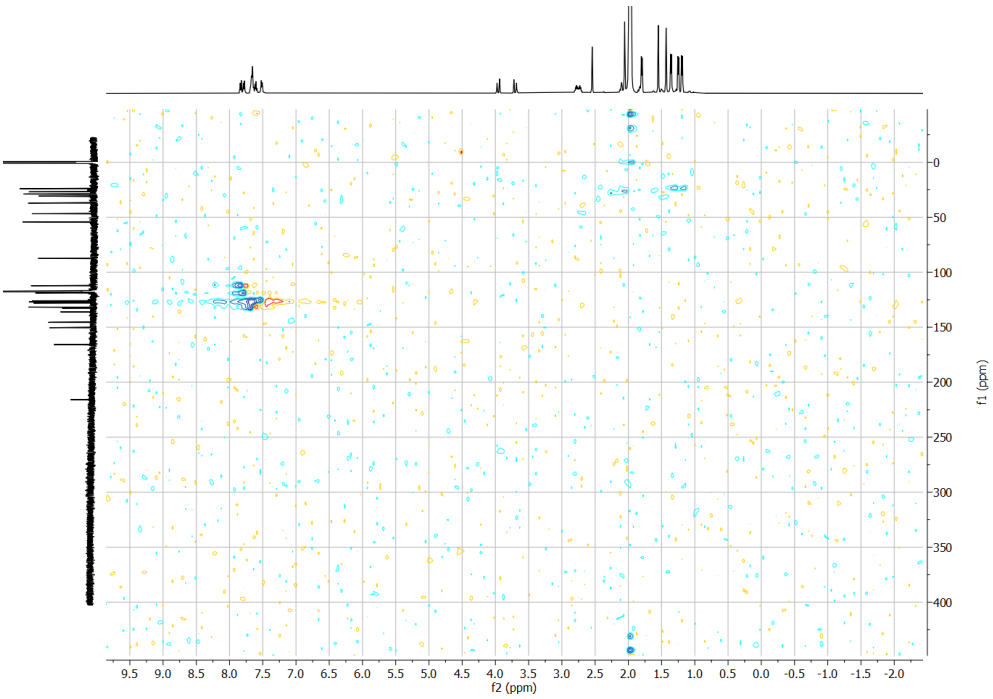

Figure S19. (^{1}H -^{13}C) HSQC NMR spectrum (500 MHz) of **5** in CD_3CN.

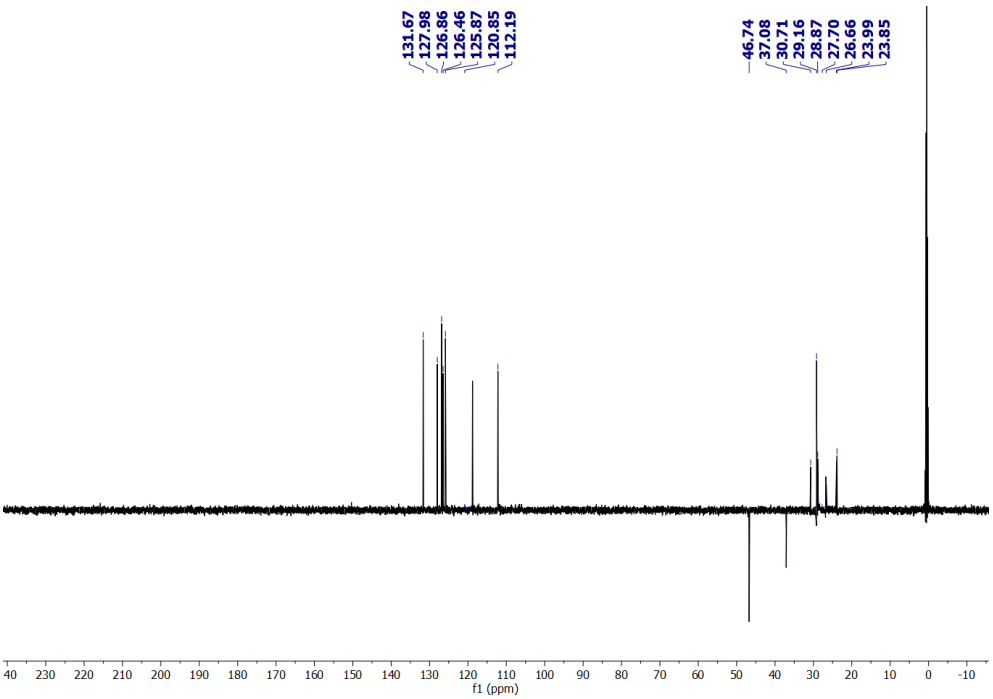

Figure S20. DEPT-^{13}C NMR spectrum (101 MHz) of **5** in CD_3CN.

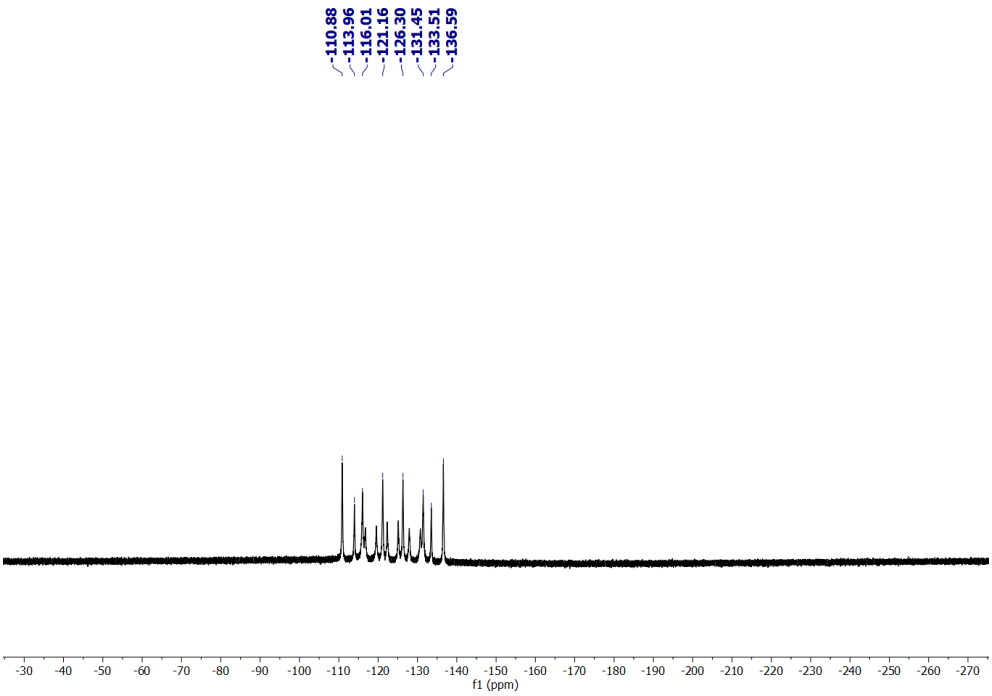

Figure S21. ^{19}F NMR spectrum (376 MHz) of **5** in CD_3CN.

Table S1: Optimization table for the Buchwald-Hartwig C-N cross-coupling catalysis.

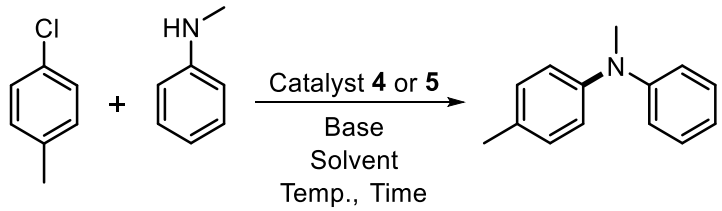

Entry	Catalyst (mol%)	Solvent	Base	Temperature (°C)	Yield (%)	Time (h)
1.	0.5	Toluene	NaO^{t}Bu	60	<1	24
2.	0.5	Toluene	K_2CO_3	60	<1	24
3.	0.5	Toluene	K_2CO_3	100	15	24
4.*	**0.5 (0.25)**	**Toluene**	**NaO^{t}Bu**	**100 (75)**	**91 (93)**	**6 (5)**
5.	0.25	Toluene	NaO^{t}Bu	100	74	24
6.	0.5	THF	NaO^{t}Bu	100	85	24
7.	0.5	DMF	NaO^{t}Bu	100	<1	24

Aryl/heteroaryl halide (1.0 equiv); Amine (1.1 equiv); NaOtBu (1.1 equiv); Toluene (3 mL).
*The values given in parenthesis in entry 4 are for the precatalyst **5**.

General procedure for the Buchwald-Hartwig Catalysis.

A 25 mL Teflon-stoppered storage flask fitted with a magnetic bar was charged with the aryl chloride/bromide (1.0 mmol), the aliphatic or aromatic primary or secondary amine (1.1 mmol), NaO^{t}Bu (1.1 mmol), **4** (0.5 mol% w.r.t. Pd) or **5** (0.25 mol% w.r.t. Pd) as the precatalyst, and 3mL of toluene. The mixture was then heated at 100 °C (for **4**) and 75 °C (for **5**) under constant stirring for 1-10 h and the reaction progress was monitored by taking aliquots. Upon completion, the reaction mixture was cooled to room temperature and filtered through a short pad of celite. 10 mL of water was added to the filtrate and the organics were extracted using EtOAc. The organic layer was dried over anhydrous $MgSO_4$ and filtered. Volatiles were removed from the filtrate to obtain the crude product, which was further purified by flash column chromatography.

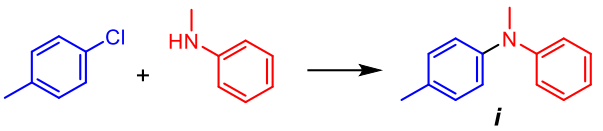

4:	0.179 g (1.41 mmol)	0.164 g (1.53 mmol)	0.253 g (1.28 mmol)
5:	0.353 g (2.79 mmol)	0.331 g (3.09 mmol)	0.511 g (2.59 mmol)

^{1}H NMR (400 MHz, $CDCl_3$): δ 7.22 (dd, *J* = 8.7, 7.3 Hz, 2H, Ar-*H*), 7.13 – 7.07 (m, 2H, Ar-*H*), 6.99 (d, *J* = 8.4 Hz, 2H, Ar-*H*), 6.94 – 6.89 (m, 2H, Ar-*H*), 6.89 – 6.84 (m, 1H, Ar-*H*), 3.28 (s, 3H, Ar-C*H*$_3$), 2.31 (s, 3H, N-C*H*$_3$). ^{13}C{^{1}H} NMR (101 MHz, $CDCl_3$) δ 149.4, 146.6, 132.0, 129.9, 129.0, 122.6, 119.8, 118.2, 40.3, 20.7. HRMS-(m/z): [M] calc. for [$C_{14}H_{15}N$], 197.1204; found, 197.1211.[4] Yields: 91% (**4**) / 93% (**5**).

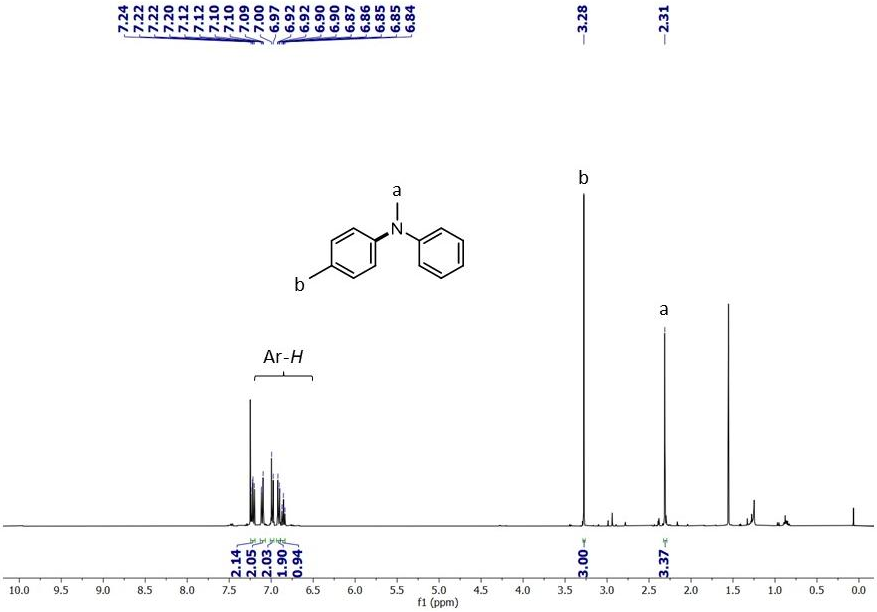

Figure-S22. ^{1}H NMR spectrum (400 MHz) of ***i*** in $CDCl_3$.

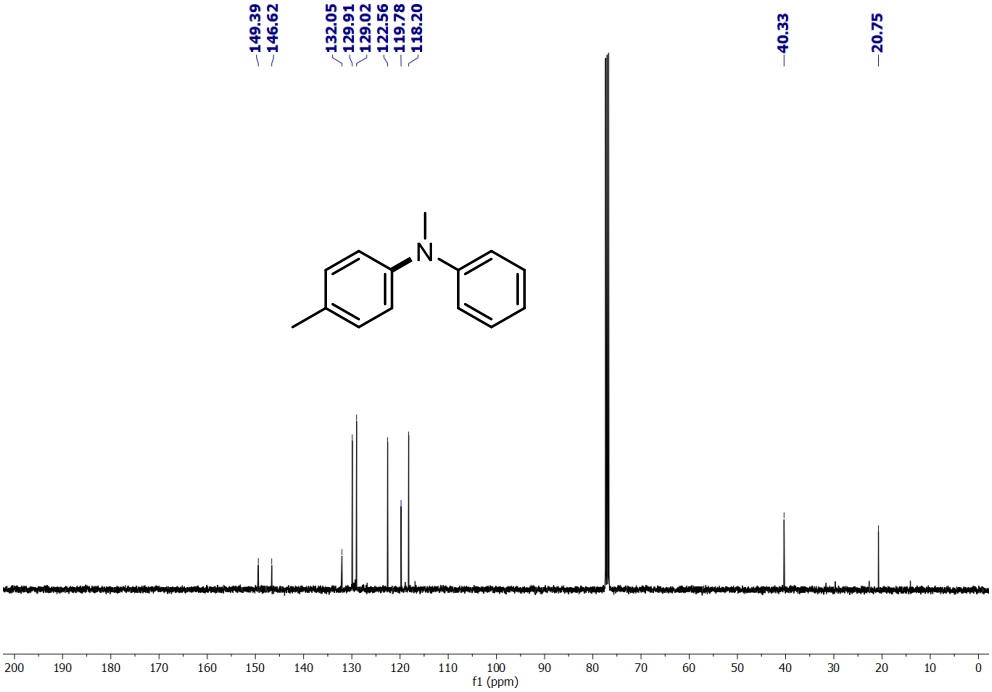

Figure-S23. ^{13}C{^{1}H} NMR spectrum (101 MHz) of ***i*** in $CDCl_3$.

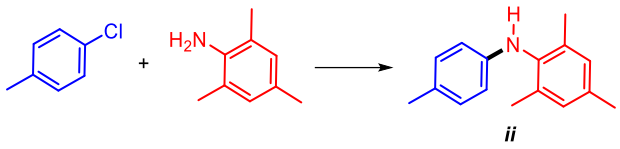

ii

4:	0.178 g (1.41 mmol)	0.207 g (1.53 mmol)	0.273 g (1.21 mmol)
5:	0.353 g (2.79 mmol)	0.418 g (3.09 mmol)	0.507 g (2.25 mmol)

^{1}H NMR (400 MHz, $CDCl_3$): δ 6.97 – 6.92 (m, 2H, Ar-*H*), 6.92 – 6.87 (m, 2H, Ar-*H*), 6.40 (d, *J* = 8.4 Hz, 2H, Ar-*H*), 5.00 (s, 1H, N*H*), 2.29 (s, 3H, CH_3), 2.23 (s, 3H, *o*-CH_3), 2.15 (d, *J* = 0.7 Hz, 6H, *p*-CH_3). ^{13}C{^{1}H} NMR (101 MHz, $CDCl_3$) δ 144.3, 136.1, 135.7, 135.1, 129.8, 129.3, 127.2, 113.5, 21.0, 20.5, 18.3. HRMS-(m/z): [M] calc. for [$C_{16}H_{19}N$], 225.1517; found, 225.1521.[5] Yields: 86% (**4**) / 81% (**5**).

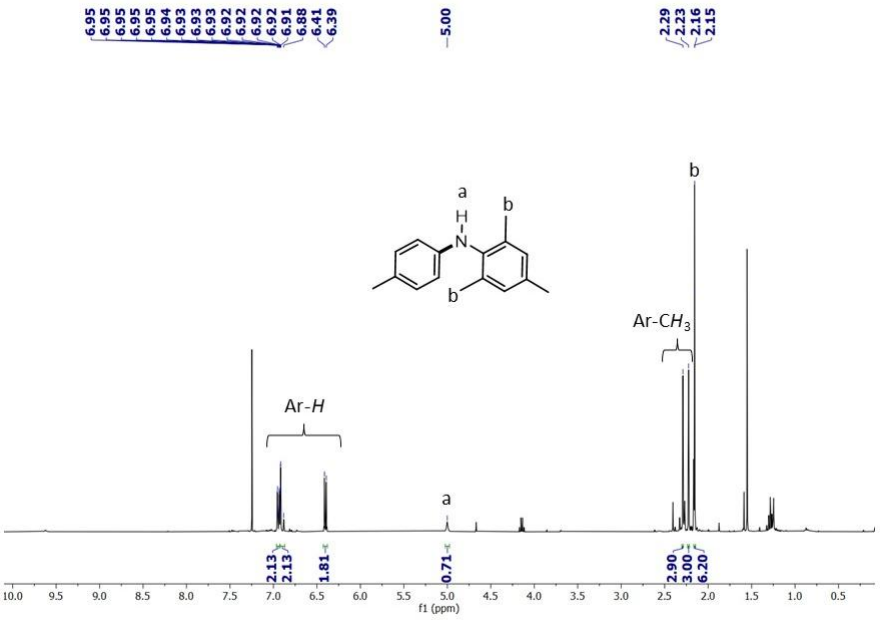

Figure-S24. ^{1}H NMR spectrum (400 MHz) of ***ii*** in $CDCl_3$.

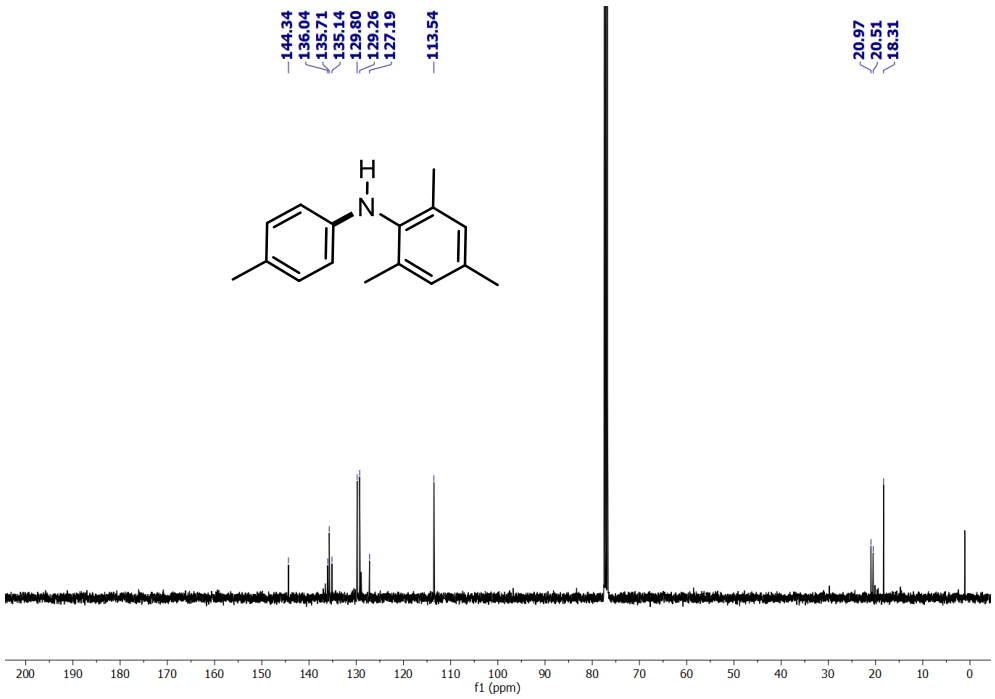

Figure-S25. ^{13}C{^{1}H} NMR spectrum (101 MHz) of ***ii*** in $CDCl_3$.

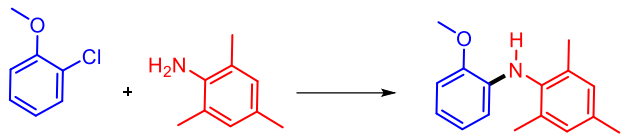

iii

4:	0.201 g (1.41 mmol)	0.207 g (1.53 mmol)	0.275 g (1.14 mmol)
5:	0.398 g (2.79 mmol)	0.418 g (3.09 mmol)	0.565 g (2.34 mmol)

^{1}H NMR (400 MHz, $CDCl_3$): δ 6.94 – 6.92 (m, 2H, Ar-*H*), 6.84 (dd, *J* = 7.5, 1.8 Hz, 1H, Ar-*H*), 6.74 – 6.65 (m, 2H, Ar-*H*), 6.12 (dd, *J* = 7.4, 2.0 Hz, 1H, Ar-*H*), 5.57 (s, 1H, N*H*), 3.93 (s, 3H, O-CH_3), 2.30 (s, 3H, *p*-CH_3), 2.16 (s, 6H, *o*-CH_3). ^{13}C{^{1}H} NMR (101 MHz, $CDCl_3$) δ 146.8, 136.4, 136.1, 135.8, 135.3, 129.2, 121.2, 117.1, 111.0, 109.9, 55.7, 21.0, 18.2. HRMS-(m/z): [M] calc. for [$C_{16}H_{19}NO$], 241.1467; found, 241.1469.[6] Yields: 81% (**4**) / 84% (**5**).

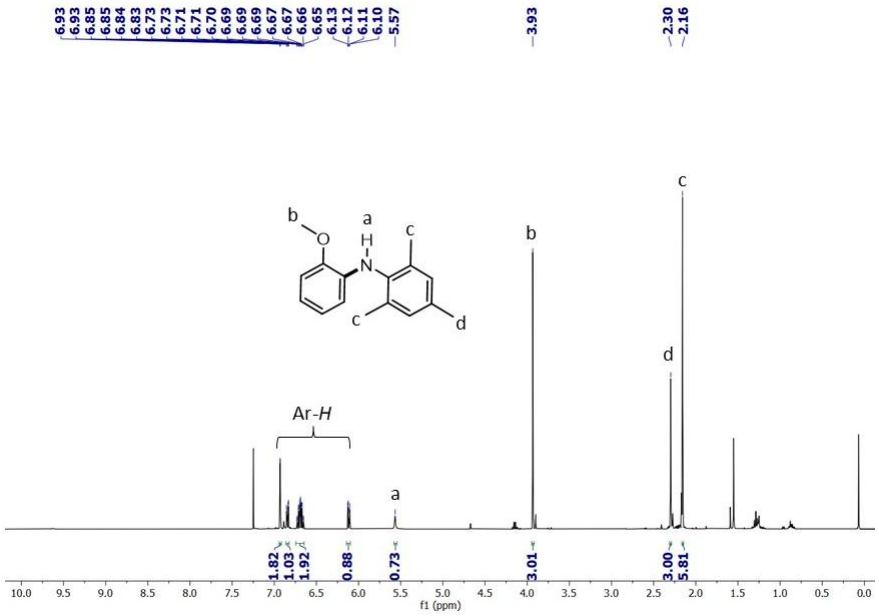

Figure-S26. ^{1}H NMR spectrum (400MHz) of ***iii*** in $CDCl_3$.

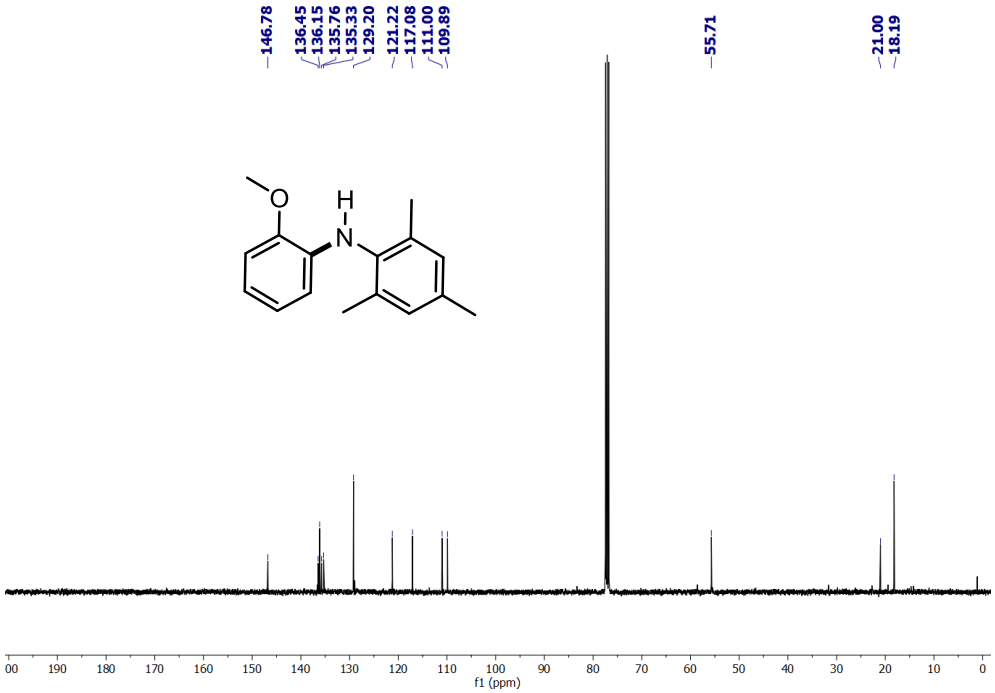

Figure-S27. ^{13}C{^{1}H} NMR spectrum (101 MHz) of ***iii*** in $CDCl_3$.

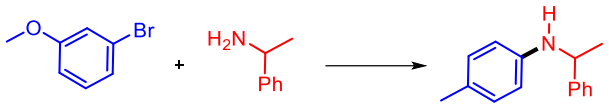

iv

4:	0.264 g (1.41 mmol)	0.185 g (1.53 mmol)	0.293 g (1.29 mmol)
5:	0.522 g (2.79 mmol)	0.374 g (3.09 mmol)	0.588 g (2.59 mmol)

^{1}H NMR (400 MHz, $CDCl_3$): δ 7.40 – 7.29 (m, 4H, Ar-*H*), 7.26 – 7.21 (m, 1H, Ar-*H*), 7.01 (t, *J* = 8.1 Hz, 1H, Ar-*H*), 6.19 (d, 2H, Ar-*H*), 6.07 (s, 1H, Ar-*H*), 4.49 (q, *J* = 6.7 Hz, 1H, N*H*CH), 4.06 (s, 1H, NHC*H*), 3.69 (s, 3H, O-CH_3), 1.52 (d, *J* = 6.7 Hz, 3H, CH_3). ^{13}C{^{1}H} NMR (126 MHz, $CDCl_3$) δ 160.6, 148.7, 145.2, 129.8, 128.6, 126.8, 125.8, 106.4, 102.4, 99.3, 54.9, 53.5, 24.9. HRMS-(m/z): [M] calc. for [$C_{15}H_{17}NO$], 227.1310; found, 227.1321.[7] Yields: 92% (**4**) / 93% (**5**).

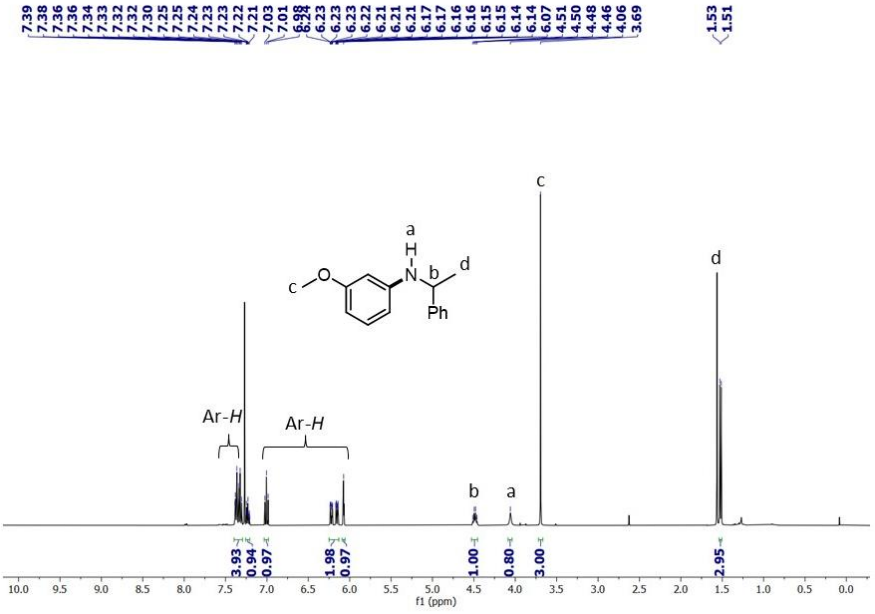

Figure-S28. ^{1}H NMR spectrum (400 MHz) of ***iv*** in $CDCl_3$.

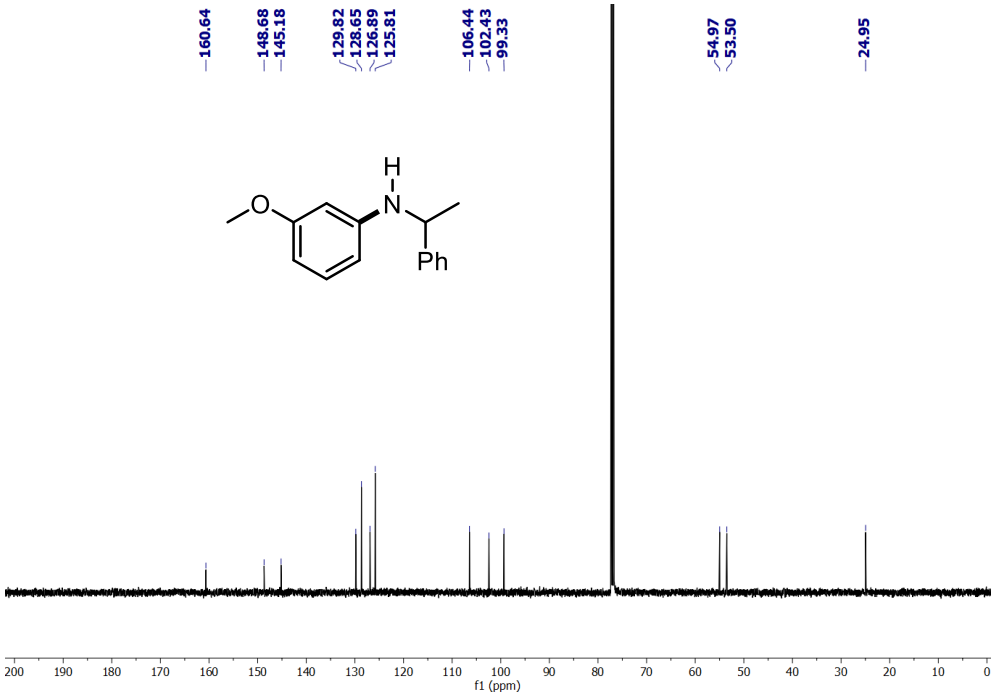

Figure-S29. ^{13}C{^{1}H} NMR spectrum (126 MHz) of ***iv*** in $CDCl_3$.

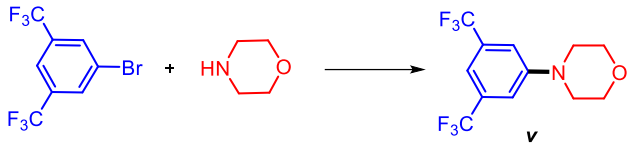

v

4:	0.413 g (1.41 mmol)	0.133 g (1.53 mmol)	0.395 g (1.32 mmol)
5:	0.817 g (2.79 mmol)	0.269 g (3.09 mmol)	0.751 g (2.51 mmol)

^{1}H NMR (400 MHz, $CDCl_3$): δ 7.31 – 7.28 (m, 1H, Ar-*H*), 7.23 – 7.21 (m, 2H, Ar-*H*), 3.89 – 3.84 (m, 4H, O-C*H*$_2$), 3.26 – 3.22 (m, 4H, N-C*H*$_2$). ^{13}C{^{1}H} NMR (101 MHz, $CDCl_3$) δ 151.7, 132.6, 132.3, 114.4, 112.5, 66.5, 48.3. ^{19}F NMR (377 MHz, $CDCl_3$) δ -63.06. HRMS-(m/z): [M] calc. for [$C_{12}H_{11}F_6NO$], 299.0745; found, 299.0763.[8] Yields: 94% (**4**) / 90% (**5**).

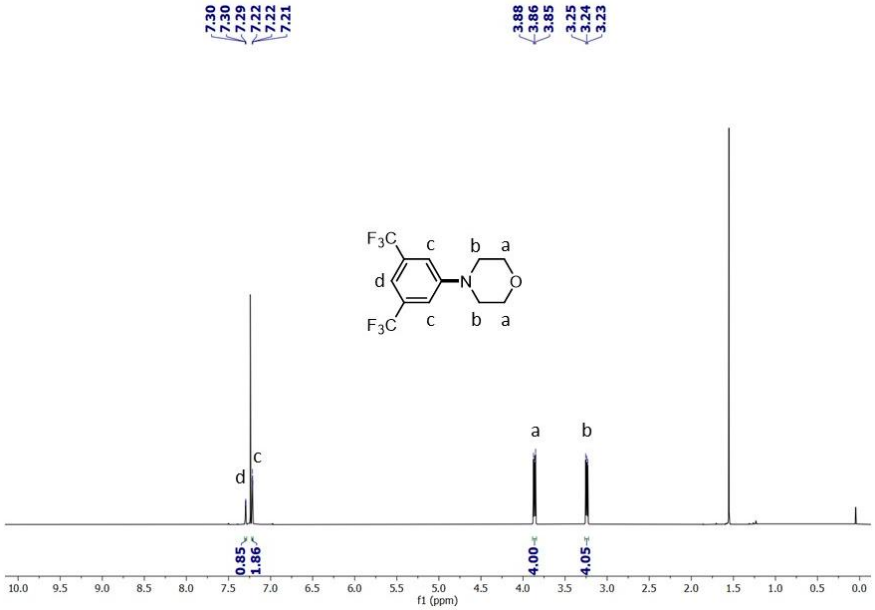

Figure-S30. ^{1}H NMR spectrum (400MHz) of ***v*** in $CDCl_3$.

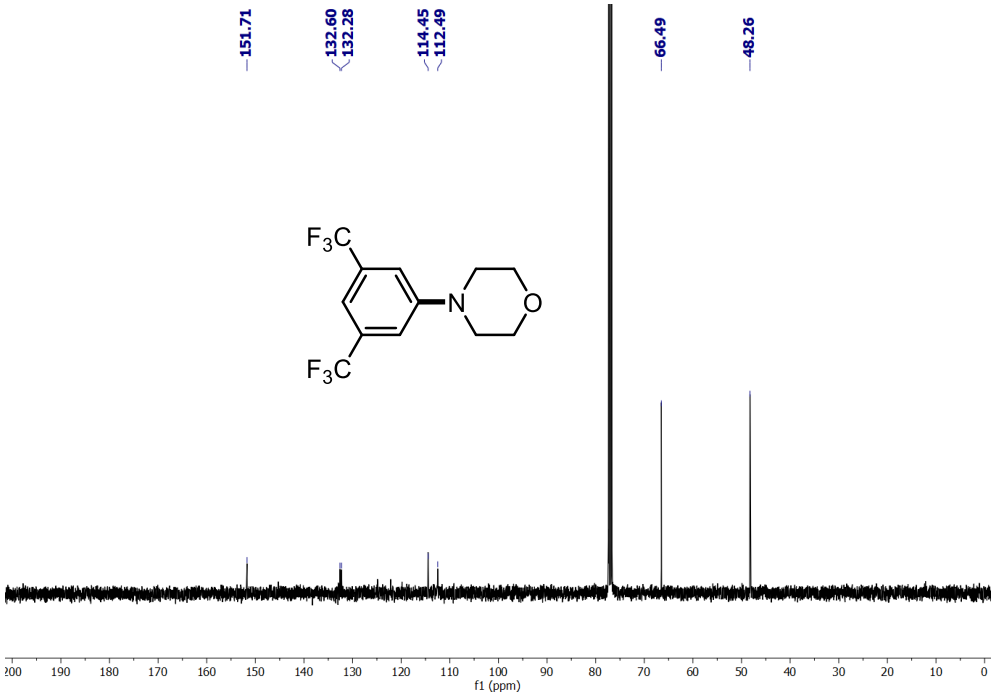

Figure-S31. ^{13}C{^{1}H} NMR spectrum (101 MHz) of ***v*** in $CDCl_3$.

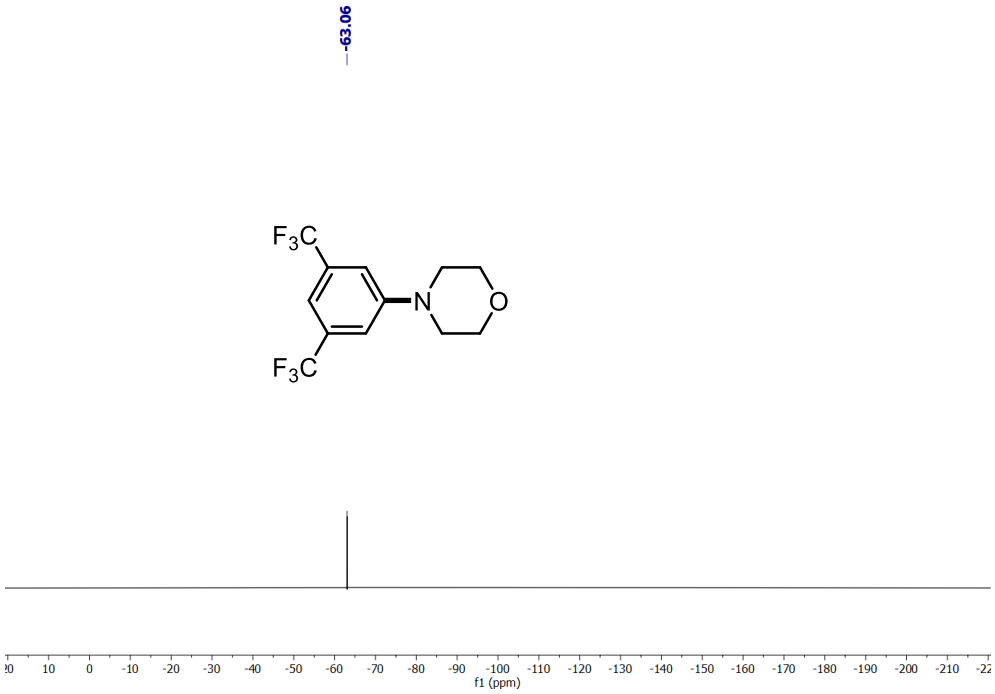

Figure-S32. ^{19}F NMR spectrum (377 MHz) of ***v*** in $CDCl_3$.

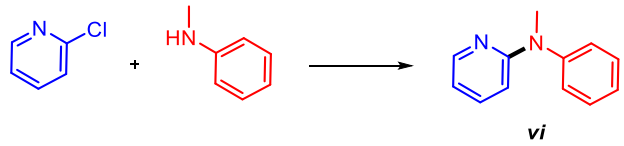

vi

4:	0.160 g (1.41 mmol)	0.164 g (1.53 mmol)	0.230 g (1.25 mmol)
5:	0.317 g (2.79 mmol)	0.331 g (3.09 mmol)	0.462 g (2.51 mmol)

^1H NMR (400 MHz, $CDCl_3$) δ 8.40 – 8.19 (m, 1H, Ar-*H*), 7.49 (d, *J* = 1.1 Hz, 1H, Ar-*H*), 7.42 – 7.34 (m, 2H, Ar-*H*), 7.30 (m, 1H, Ar-*H*), 7.28 – 7.25 (m, 1H, Ar-*H*), 7.23 – 7.16 (m, 1H, Ar-*H*), 6.59 (t, 1H, Ar-*H*), 6.52 (d, 1H, Ar-*H*), 3.47 (s, 3H, C*H*$_3$). $^{13}C\{^1H\}$ NMR (126 MHz, $CDCl_3$) δ 150.3, 147.8, 136.6, 129.7, 126.3, 125.4, 122.6, 113.1, 109.2, 38.4. HRMS-(m/z): [M] calc. for [$C_{12}H_{12}N_2$], 184.1000; found, 184.1013.[9] Yields: 89% (**4**) / 90% (**5**).

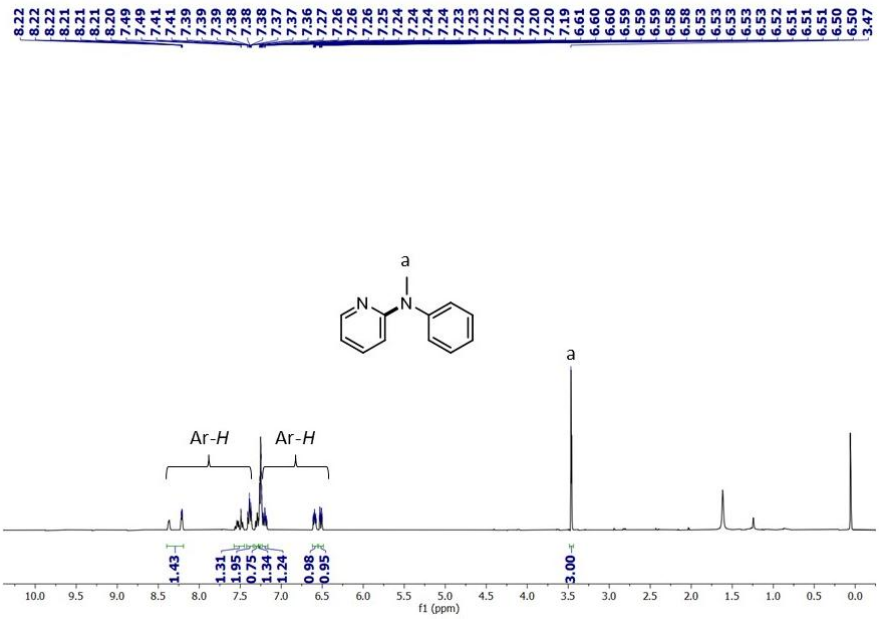

Figure-S33. ^1H NMR spectrum (400 MHz) of ***vi*** in $CDCl_3$.

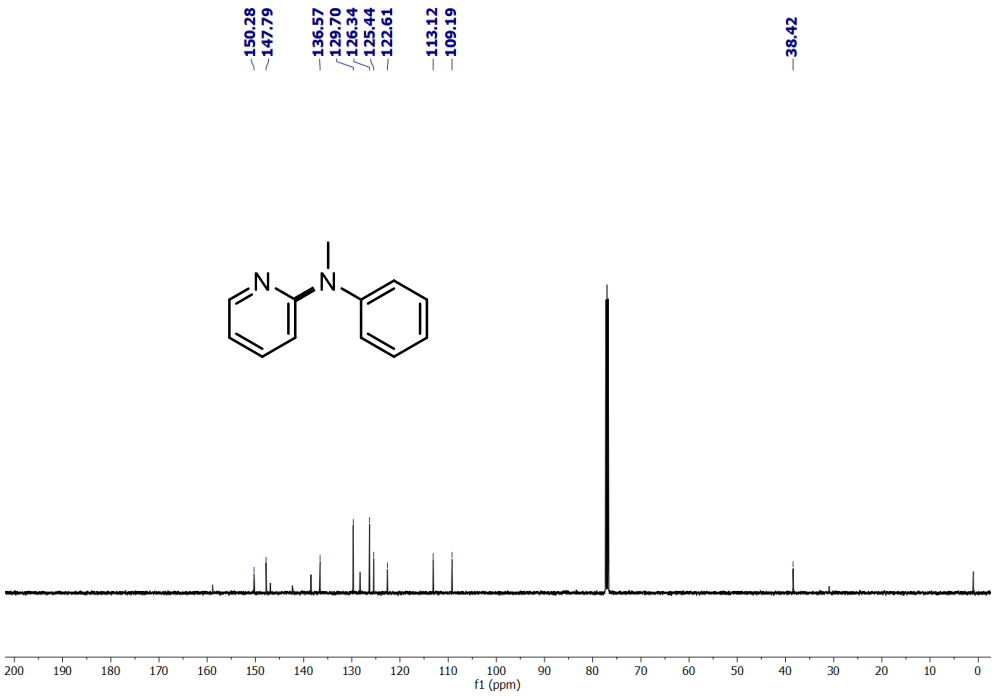

Figure-S34. $^{13}C\{^{1}H\}$ NMR spectrum (126 MHz) of ***vi*** in $CDCl_3$.

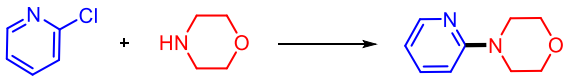

vii

4:	0.160 g (1.41 mmol)	0.133 g (1.53 mmol)	0.218 g (1.33 mmol)
5:	0.317 g (2.79 mmol)	0.269 g (3.09 mmol)	0.415 g (2.53 mmol)

^{1}H NMR (400 MHz, $CDCl_3$) δ 8.18 (dd, *J* = 4.9, 2.0, 0.9 Hz, 1H, Ar-*H*), 7.47 (dd, *J* = 8.5, 7.2, 2.0 Hz, 1H, Ar-*H*), 6.67 – 6.58 (m, 2H, Ar-*H*), 3.83 – 3.77 (m, 4H, O-CH_2), 3.51 – 3.43 (m, 4H, N-CH_2). $^{13}C\{^{1}H\}$ NMR (101 MHz, $CDCl_3$) δ 159.7, 148.1, 137.6, 113.9, 107.1, 66.9, 45.7. HRMS-(m/z): [M] calc. for [$C_9H_{12}N_2O$], 164.0950; found, 164.0952.[10] Yields: 95% (**4**) / 91% (**5**).

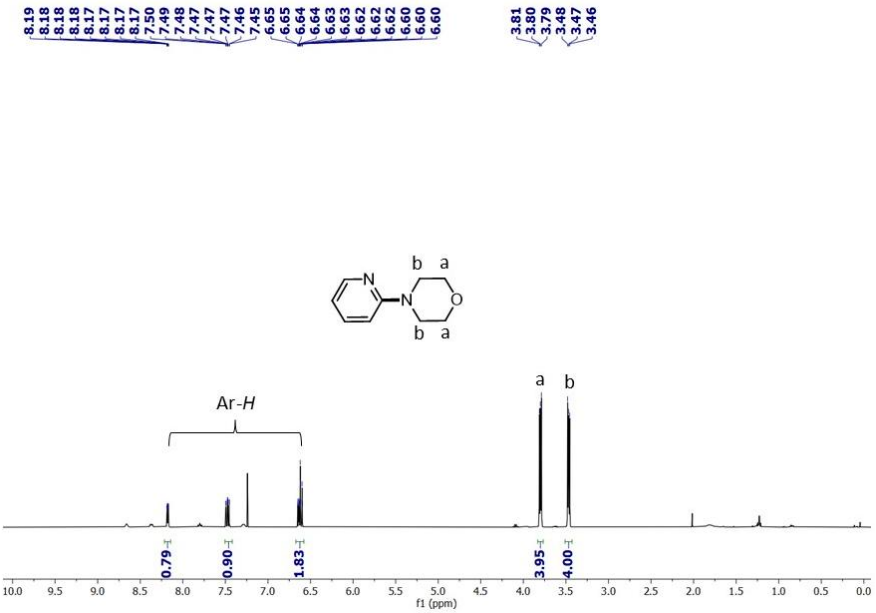

Figure-S35. ^{1}H NMR spectrum (400 MHz) of ***vii*** in $CDCl_3$.

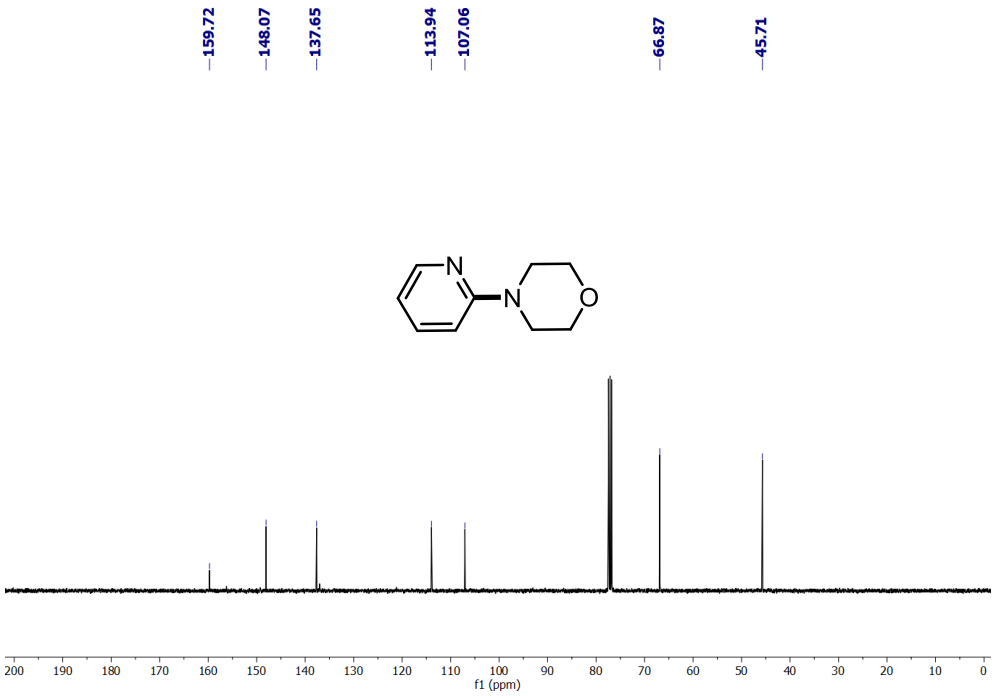

Figure-S36. $^{13}C\{^{1}H\}$ NMR spectrum (101 MHz) of ***vii*** in $CDCl_3$.

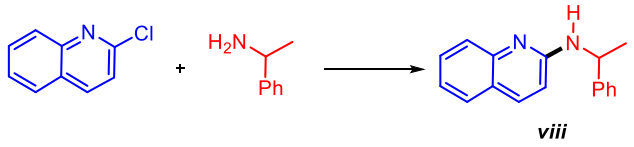

viii

4:	0.231 g (1.41 mmol)	0.185 g (1.53 mmol)	0.320 g (1.29 mmol)
5:	0.456 g (2.79 mmol)	0.374 g (3.09 mmol)	0.616 g (2.48 mmol)

^{1}H NMR (400 MHz, $CDCl_3$) δ 7.75 (dd, *J* = 8.9, 0.8 Hz, 1H, Ar-*H*), 7.69 – 7.63 (m, 1H, Ar-*H*), 7.57 – 7.49 (m, 2H, Ar-*H*), 7.44 – 7.40 (m, 2H, Ar-*H*), 7.35 – 7.30 (m, 2H, Ar-*H*), 7.24 – 7.16 (m, 1H, Ar-*H*), 6.53 (d, *J* = 8.9 Hz, 1H, Ar-*H*), 5.21 (d, *J* = 6.8 Hz, 1H, N*H*CH), 5.09 (q, *J* = 6.7 Hz, 1H, NHC*H*), 1.61 (d, *J* = 6.8 Hz, 3H, C*H*$_3$). $^{13}C\{^{1}H\}$ NMR (126 MHz, $CDCl_3$) δ 156.4, 148.0, 144.7, 137.6, 129.6, 128.7, 127.5, 127.1, 126.1, 123.5, 122.1, 110.7, 51.4, 23.8. HRMS-(m/z): [M] calc. for [$C_{17}H_{16}N_2$], 248.1313; found, 248.1314. Yields: 92% (**4**) / 89% (**5**).

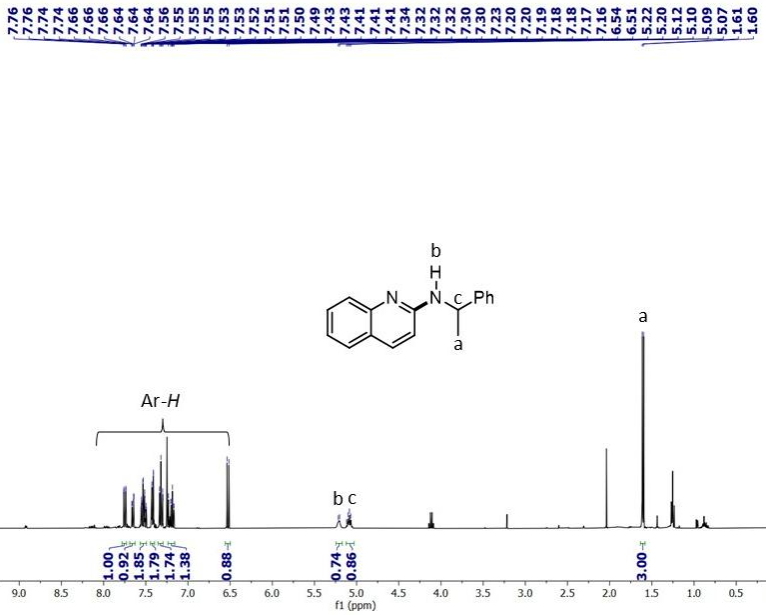

Figure-S37. ^{1}H NMR spectrum (400 MHz) of ***viii*** in $CDCl_3$.

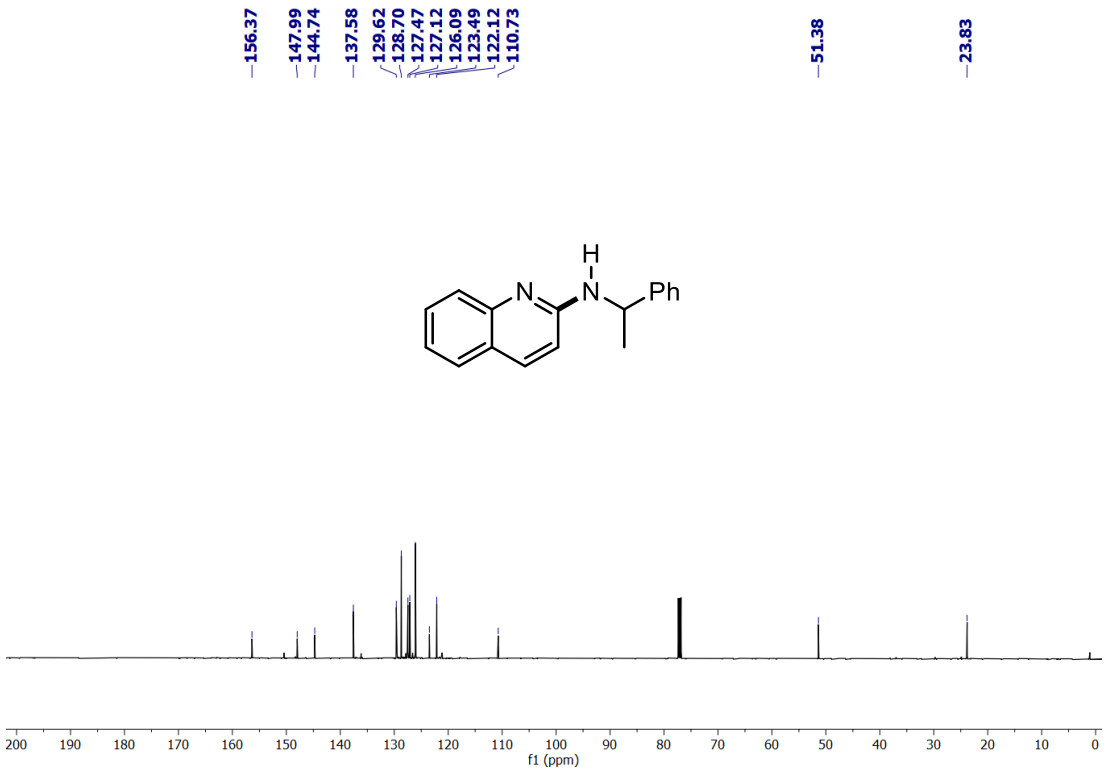

Figure-S38. $^{13}C\{^{1}H\}$ NMR spectrum (126 MHz) of ***viii*** in $CDCl_3$.

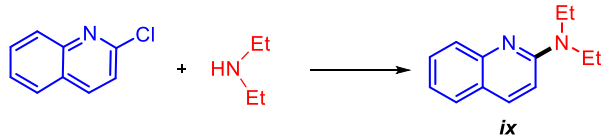

ix

4:	0.231 g (1.41 mmol)	0.112 g (1.53 mmol)	0.228 g (1.14 mmol)
5:	0.456 g (2.79 mmol)	0.226 g (3.09 mmol)	0.447 g (2.23 mmol)

^{1}H NMR (400 MHz, $CDCl_3$) δ 7.80 (dd, *J* = 9.1, 0.8 Hz, 1H, Ar-*H*), 7.63 (d, 1H, Ar-*H*), 7.56 – 7.51 (m, 1H, Ar-*H*), 7.50 – 7.43 (m, 1H, Ar-*H*), 7.12 (dd, *J* = 8.0, 6.9, 1.2 Hz, 1H, Ar-*H*), 6.81 (d, *J* = 9.2 Hz, 1H, Ar-*H*), 3.64 (q, *J* = 7.1 Hz, 4H, N-C*H*$_2$-CH$_3$), 1.22 (t, *J* = 7.1 Hz, 6H, N-CH$_2$-C*H*$_3$). $^{13}C\{^{1}H\}$ NMR (126 MHz, $CDCl_3$) δ 156.0, 148.6, 148.5, 136.9, 130.5, 129.2, 127.1, 126.3, 121.2, 109.1, 42.4, 13.3. HRMS-(m/z): [M] calc. for [$C_{13}H_{16}N_2$], 200.1313; found, 200.1318.[11] Yields: 85% (**4**) / 87% (**5**).

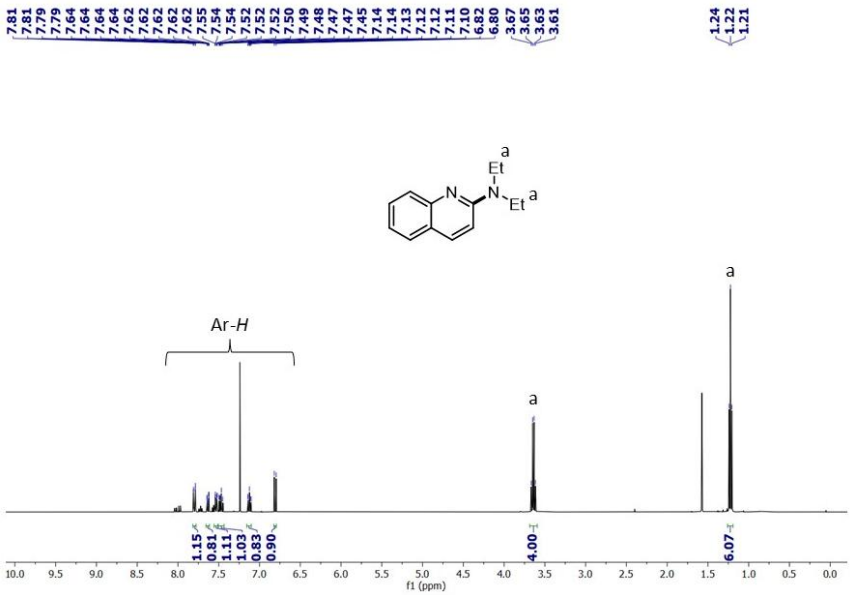

Figure-S39. ^{1}H NMR spectrum (400 MHz) of ***ix*** in $CDCl_3$.

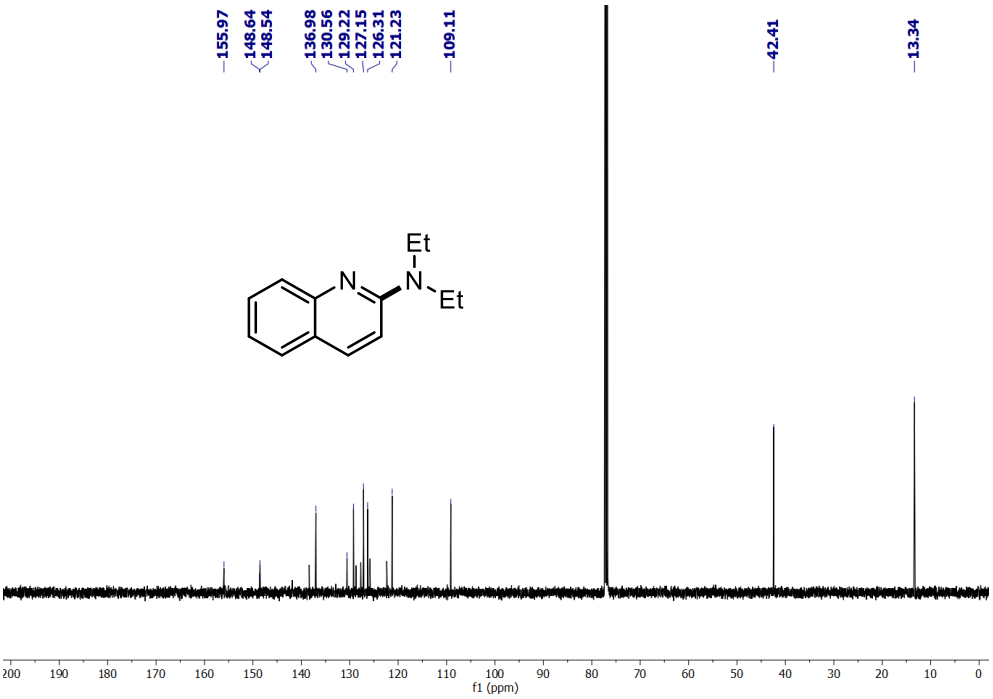

Figure-S40. $^{13}C\{^{1}H\}$ NMR spectrum (126 MHz) of ***ix*** in $CDCl_3$.

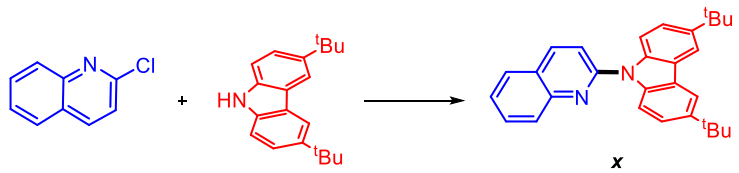

x

4:	0.231 g (1.41 mmol)	0.427 g (1.53 mmol)	0.476 g (1.17 mmol)
5:	0.456 g (2.79 mmol)	0.862 g (3.09 mmol)	0.907 g (2.23 mmol)

^{1}H NMR (400 MHz, $CDCl_3$) δ 8.34 – 8.27 (m, 1H, Ar-*H*), 8.18 – 8.12 (m, 3H, Ar-*H*), 7.98 (dt, *J* = 8.7, 0.7 Hz, 2H, Ar-*H*), 7.89 – 7.85 (m, 1H, Ar-*H*), 7.83 – 7.74 (m, 2H, Ar-*H*), 7.59 – 7.49 (m, 3H, Ar-*H*), 1.48 (s, 18H, ^{t}Bu-*H*). $^{13}C\{^{1}H\}$ NMR (101 MHz, $CDCl_3$) δ 151.39, 147.87, 144.32, 138.57, 137.97, 130.3, 128.8, 127.7, 126.4, 126.1, 124.8, 124.1, 117.4, 116.2, 111.4, 34.9, 32.0. HRMS-(m/z): [M] calc. for [$C_{29}H_{30}N_2$], 406.2409; found, 406.2412. Yields: 83% (**4**) / 80% (**5**).

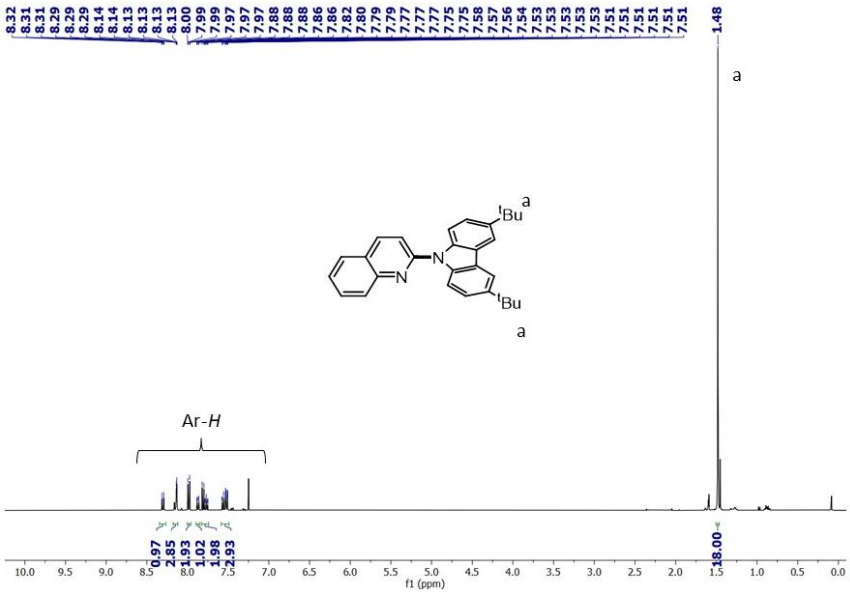

Figure-S41. ^{1}H NMR spectrum (400MHz) of ***x*** in $CDCl_3$.

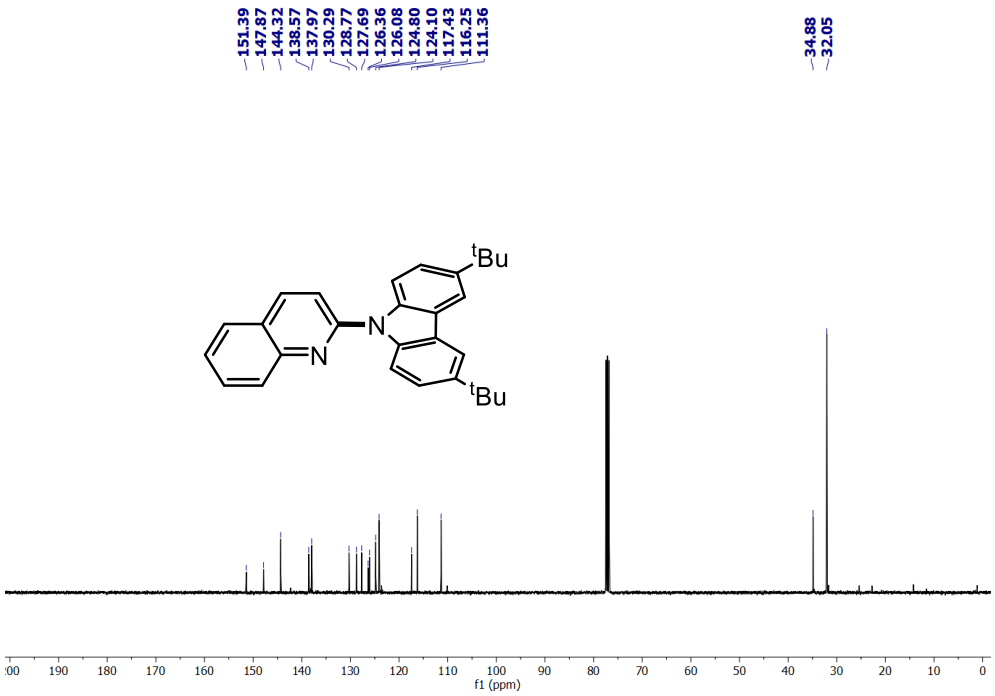

Figure-S42. $^{13}C\{^{1}H\}$ NMR spectrum (101 MHz) of ***x*** in $CDCl_3$.

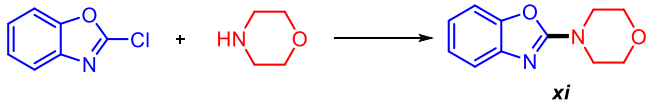

xi

4:	0.217 g (1.41 mmol)	0.133 g (1.53 mmol)	0.265 g (1.29 mmol)
5:	0.428 g (2.79 mmol)	0.269 g (3.09 mmol)	0.524 g (2.56 mmol)

^{1}H NMR (400 MHz, $CDCl_3$) δ 7.37 (dd, *J* = 8.0, 1.3 Hz, 1H, Ar-*H*), 7.25 (d, *J* = 1.1 Hz, 1H, Ar-*H*), 7.16 (td, *J* = 7.7, 1.2 Hz, 1H, Ar-*H*), 7.03 (td, *J* = 7.8, 1.3 Hz, 1H, Ar-*H*), 3.80 (dd, *J* = 6.1, 3.6 Hz, 4H, O-CH_2), 3.71 – 3.64 (m, 4H, N-CH_2). $^{13}C\{^{1}H\}$NMR (126 MHz, $CDCl_3$) δ 162.1, 148.7, 142.7, 124.1, 121.0, 116.4, 108.9, 66.2, 45.7. HRMS-(m/z): [M] calc. for [$C_{11}H_{12}N_2O_2$], 204.0899; found, 204.0901.[10] Yields: 92% (**4**) / 92% (**5**).

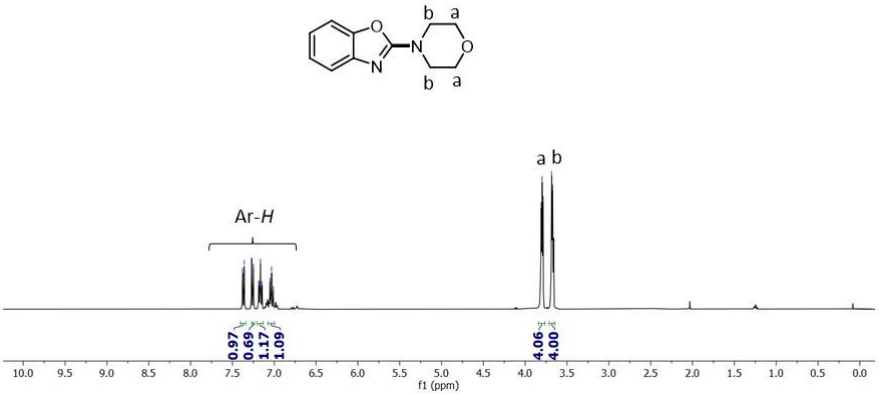

Figure-S43. ^{1}H NMR spectrum (400MHz) of ***xi*** in $CDCl_3$.

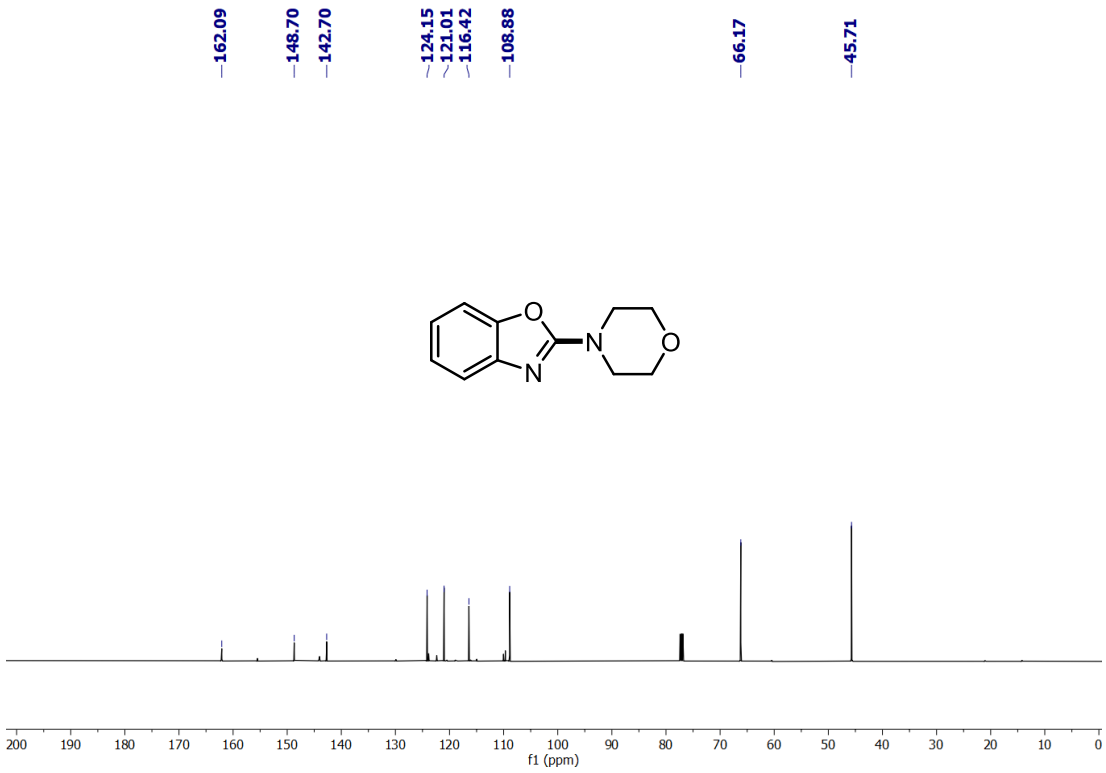

Figure-S44. $^{13}C\{^{1}H\}$ NMR spectrum (126 MHz) of ***xi*** in $CDCl_3$.

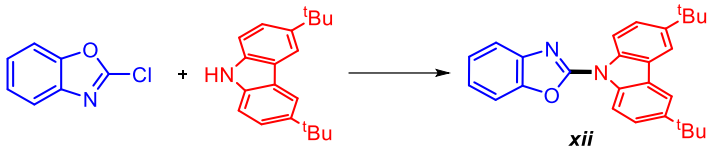

xii

4:	0.217 g (1.41 mmol)	0.427 g (1.53 mmol)	0.453 g (1.14 mmol)
5:	0.428 g (2.79 mmol)	0.863 g (3.09 mmol)	0.885 g (2.23 mmol)

^{1}H NMR (400 MHz, $CDCl_3$) d 8.54 (dd, *J* = 8.8, 0.6 Hz, 2H, Ar-*H*), 8.05 (dd, *J* = 2.1, 0.6 Hz, 2H, Ar-*H*), 7.71 (d, 1H, Ar-*H*), 7.63 – 7.57 (m, 3H, Ar-*H*), 7.35 (td, *J* = 7.6, 1.2 Hz, 1H, Ar-*H*), 7.28 (td, *J* = 7.8, 1.4 Hz, 1H, Ar-*H*), 1.46 (s, 18H, *t*Bu-*H*). $^{13}C\{^{1}H\}$ NMR (101 MHz, $CDCl_3$) d 155.9, 148.3, 146.4, 141.5, 136.4, 125.8, 124.9, 124.8, 123.3, 118.8, 116.2, 114.7, 109.9, 34.9, 31.9. HRMS-(m/z): [M] calc. for [$C_{27}H_{28}N_2O$], 396.2202; found, 396.2210. Yields: 81% (**4**) / 80% (**5**).

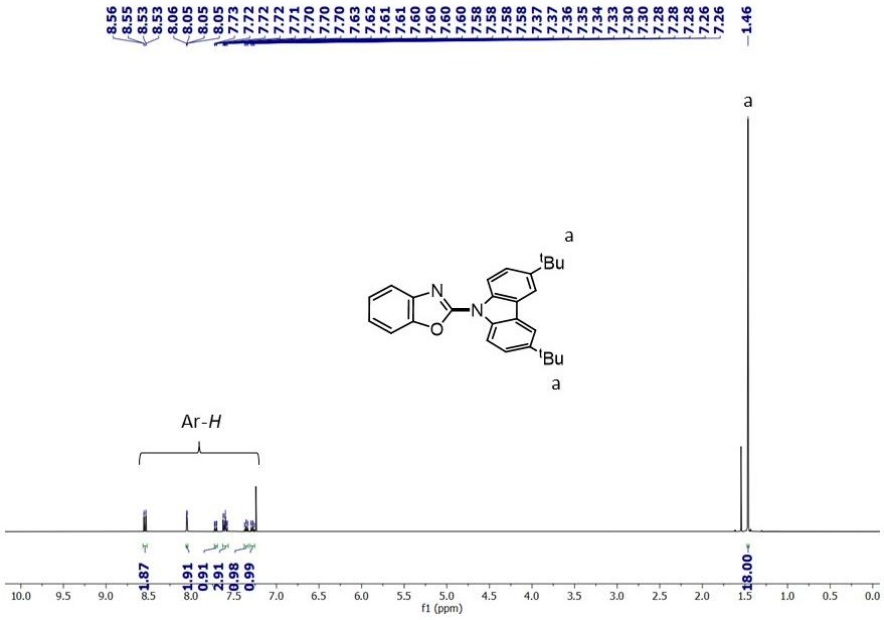

Figure-S45. ^{1}H NMR spectrum (400MHz) of ***xii*** in $CDCl_3$.

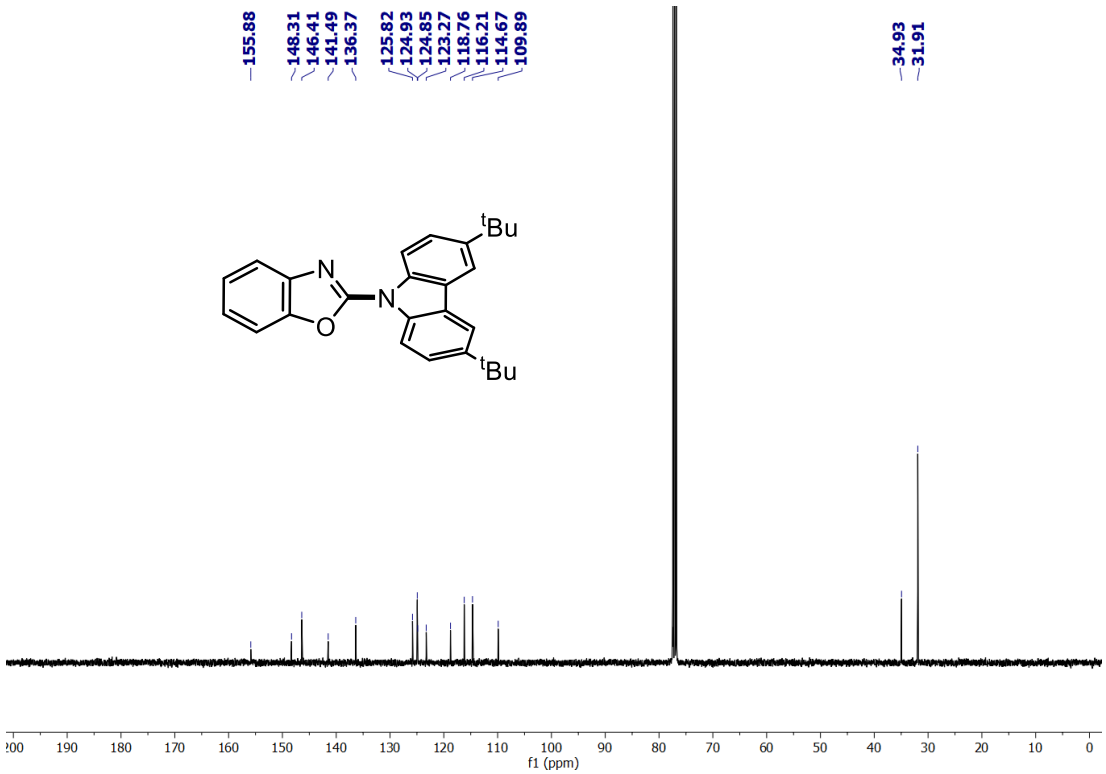

Figure-S46. $^{13}C\{^{1}H\}$ NMR spectrum (101 MHz) of ***xii*** in $CDCl_3$.

Synthetic Scheme for E':

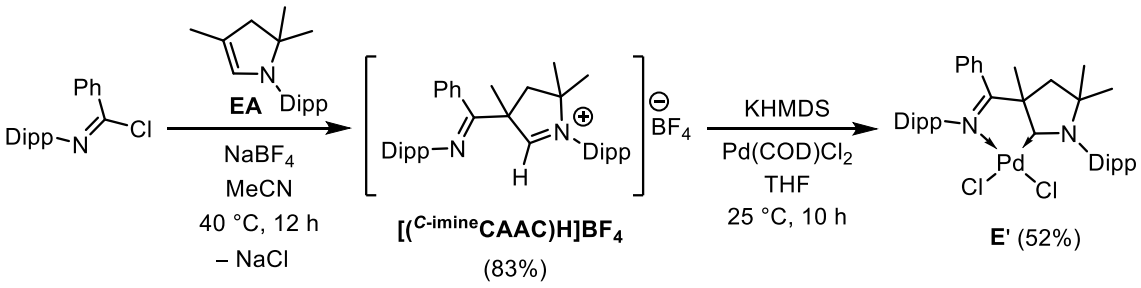

Step 1: A 100 mL Teflon-stoppered flask fitted with a magnetic bead and a J. Young-styled valve on the sidearm was charged with *N*-(2,6-diisopropylphenyl)benzimidoylchloride (0.500 g, 1.667 mmol), $NaBF_4$ (0.201 g, 1.834 mmol), and the enamine **EA** (0.452 g, 1.667 mmol). Anhydrous MeCN was then added and the reaction mixture was heated at 40 °C for 12 hours. Upon cooling down to room temperature, the volatiles were then removed under reduced pressure to obtain a crude residue. This residue was extracted with DCM, and the DCM was subsequently removed under reduced pressure to get a sticky solid. The solid was further washed with Et_2O to afford the **[($^{C\text{-imine}}$CAAC)H]BF_4** (0.861 g, 1.383 mmol, 83%) as a pale-yellow solid.

^{1}H NMR (400 MHz, $CDCl_3$) d 8.88 (s, 1H, iminium-*H*), 7.54 (t, *J* = 7.8 Hz, 1H, Ar-*H*), 7.39 (dd, *J* = 7.9, 1.4 Hz, 1H, Ar-*H*), 7.34 – 7.27 (m, 4H, Ar-*H*), 7.24 – 7.19 (m, 2H, Ar-*H*), 7.10 (dd, *J* = 7.7, 1.5 Hz, 1H, Ar-*H*), 7.03 (t, *J* = 7.7 Hz, 1H, Ar-*H*), 6.91 (dd, *J* = 7.6, 1.5 Hz, 1H, Ar-*H*), 3.33 (s, 2H, ring-CH_2), 3.05 (p, *J* = 6.8 Hz, 1H, ^{i}Pr-C*H*), 2.92 (p, *J* = 6.7 Hz, 1H, ^{i}Pr-C*H*), 2.79 (p, *J* = 6.7 Hz, 1H, ^{i}Pr-C*H*), 2.58 (p, *J* = 6.8 Hz, 1H, ^{i}Pr-C*H*), 1.89 (s, 3H, CH_3), 1.73 (s, 3H, CH_3), 1.65 (s, 3H, CH_3), 1.40 (d, *J* = 6.6 Hz, 3H, CH_3), 1.29 (d, *J* = 6.8 Hz, 3H, CH_3), 1.25 (d, *J* = 6.7 Hz, 3H, CH_3), 1.21 (d, *J* = 6.8 Hz, 3H, CH_3), 1.16 (d, *J* = 6.8 Hz, 3H, CH_3), 1.00 (d, *J* = 6.8 Hz, 3H, CH_3), 0.91 (d, *J* = 6.6 Hz, 3H, CH_3), 0.59 (d, *J* = 6.8 Hz, 3H, CH_3). ^{19}F (376 MHz, $CDCl_3$) d -151.63, -151.68 (d, *J* = 1.9 Hz). ^{11}B (128 MHz, $CDCl_3$) d -1.85. $^{13}C\{^{1}H\}$ NMR (101 MHz, $CDCl_3$) d 186.0, 175.1, 145.2, 145.2, 138.2, 134.8, 132.2, 131.5, 130.9, 129.0, 128.9, 127.9, 125.8, 125.6, 125.3, 123.7, 123.3, 84.4, 61.1, 29.9, 29.8, 29.0, 28.5, 27.9, 26.9, 26.7, 24.7, 23.8, 23.7, 23.1, 22.4, 22.2, 21.6. HRMS-(m/z): $[M]^+$ calc. for $[C_{38}H_{51}N_2]^+$, 535.4041; found, 535.4080.

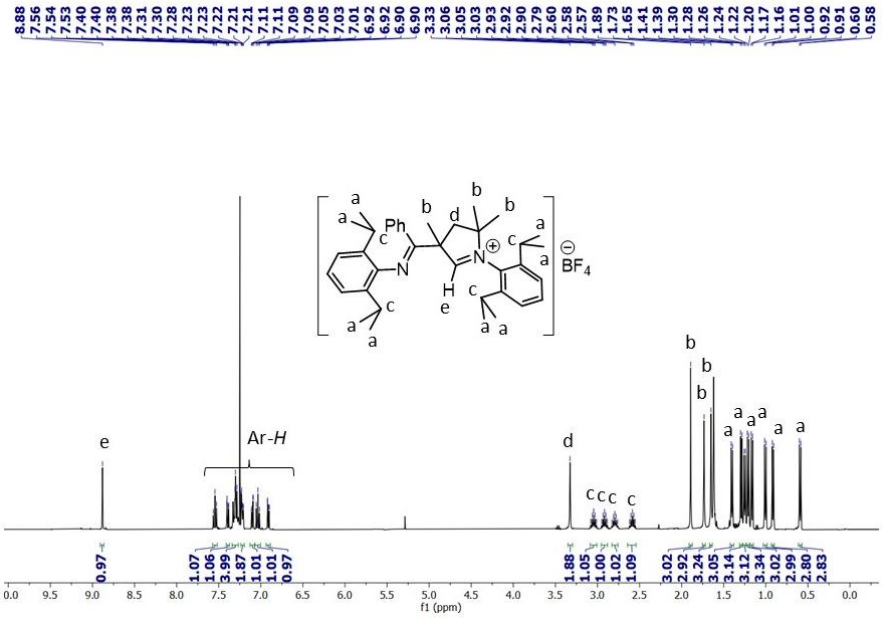

Figure-S47. ^{1}H NMR spectrum (400 MHz) of **[(*C*-imine CAAC)H]BF_4** in $CDCl_3$.

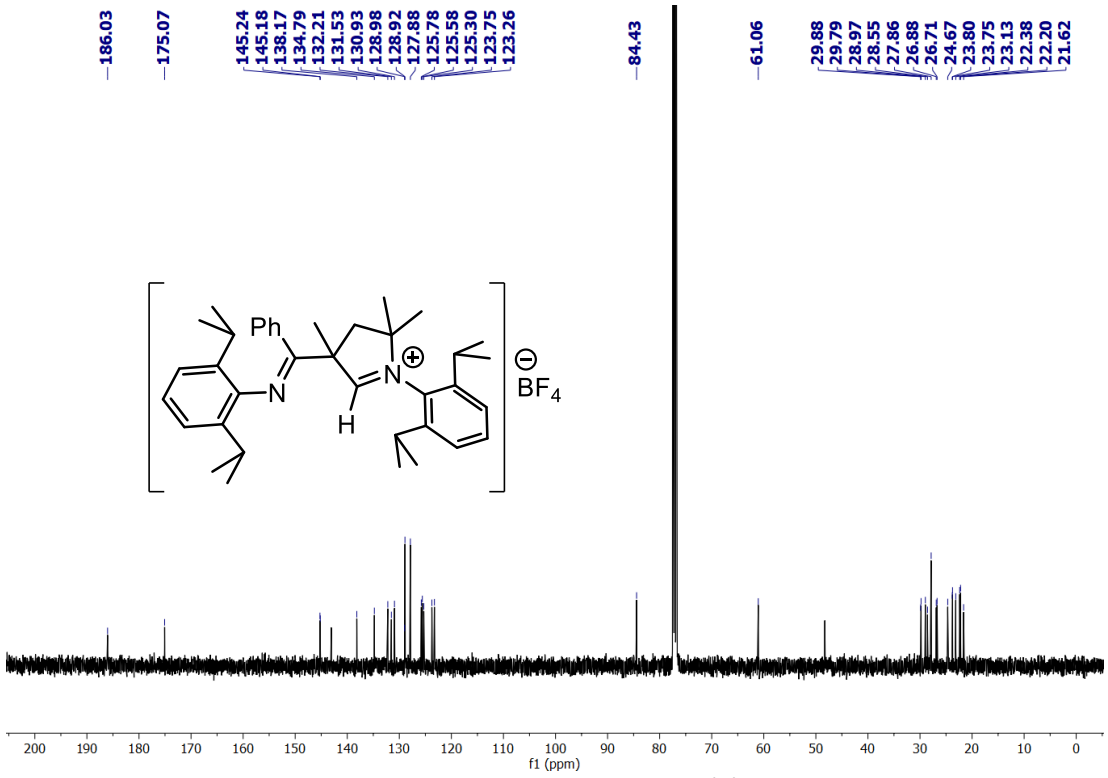

Figure-S48. $^{13}C\{^{1}H\}$ NMR spectrum (101 MHz) of **[(*C*-imine CAAC)H]BF_4** in $CDCl_3$.

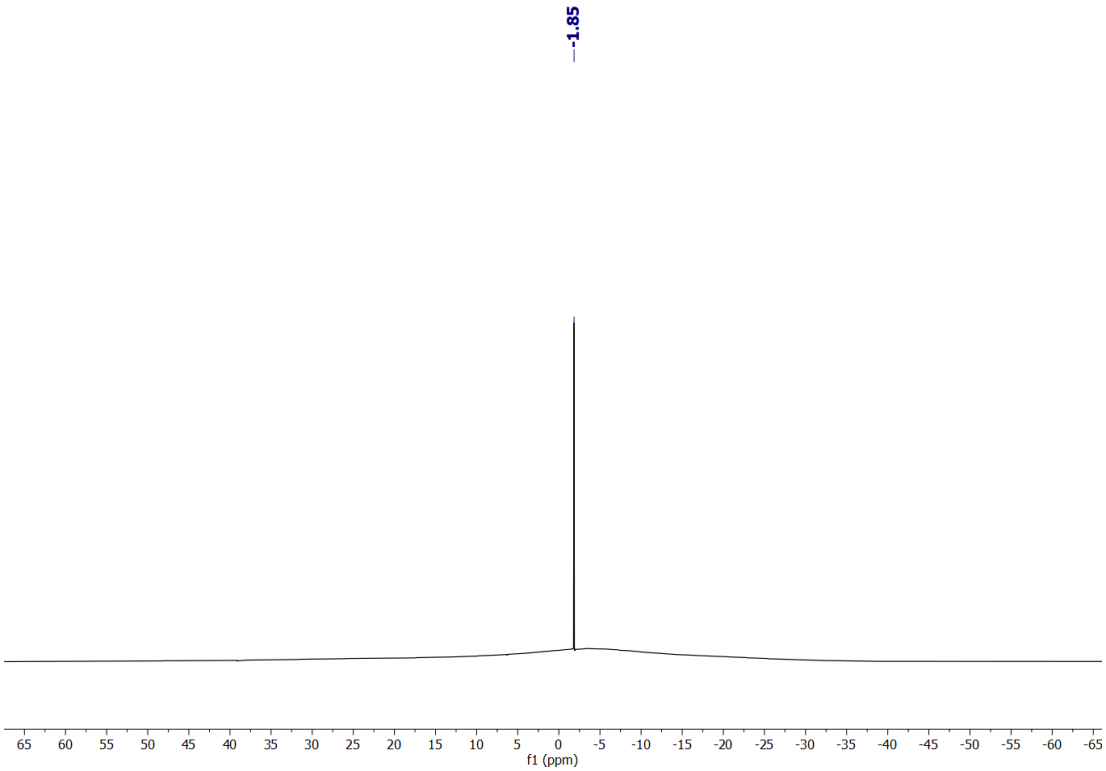

Figure S49. ^{11}B NMR spectrum (128 MHz) of **[(*C*-imine CAAC)H]BF$_4$** in $CDCl_3$.

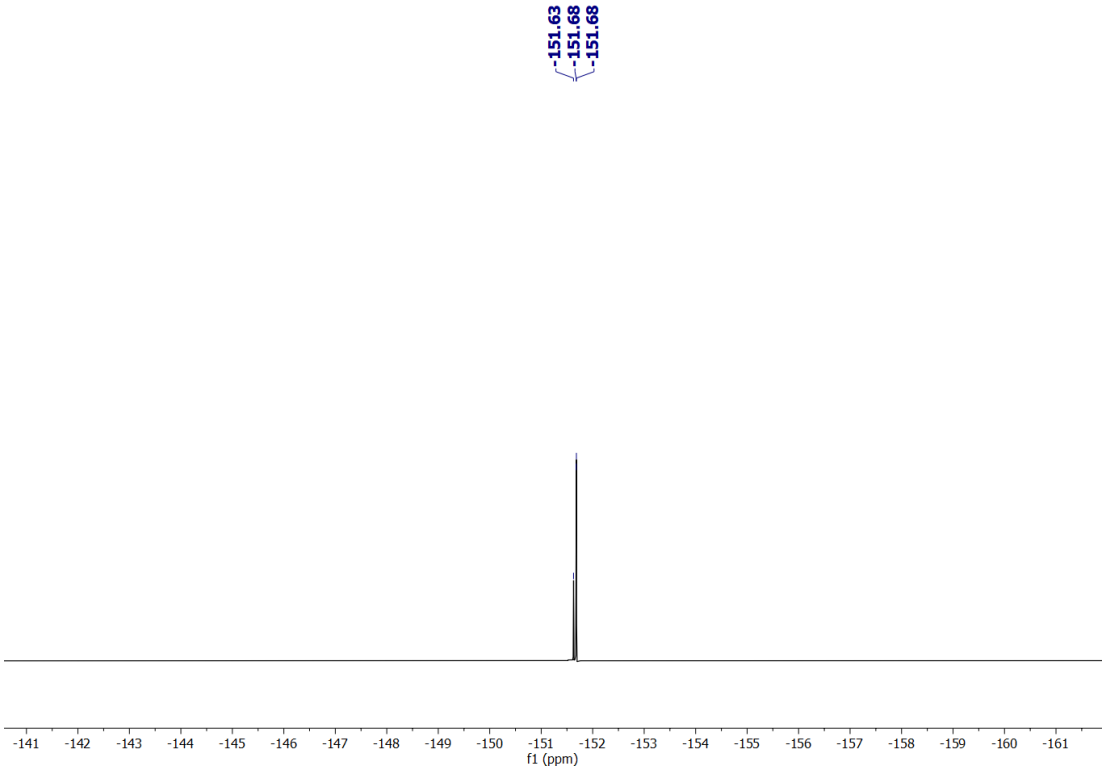

Figure S50. ^{19}F NMR spectrum (376 MHz) of **[(*C*-imine CAAC)H]BF$_4$** in $CDCl_3$.

Step 2: A 10 mL glass vial fitted with a magnetic bead was charged with **[(*C*-imine CAAC)H]BF$_4$** (0.500 g, 0.803 mmol) and KHMDS (0.160 g, 0.803 mmol) followed by 3 mL of THF. The mixture was stirred at room temperature for 10 minutes. It was then slowly added to a 2 mL THF suspension of $Pd(COD)Cl_2$ (0.229 g, 0.803 mmol) and stirred for 10 h. Volatiles were then removed under reduced pressure and the residue was extracted with DCM and further washed with THF to afford **E'** (0.297 g, 0.417 mmol, 52%) as a pale-yellow solid.

^{1}H NMR (400 MHz, CD_2Cl_2) δ 7.51 (t, *J* = 7.8 Hz, 1H, Ar-*H*), 7.46 – 7.36 (m, 2H, Ar-*H*), 7.35 – 7.19 (m, 7H, Ar-*H*), 6.95 (dd, *J* = 6.2, 2.9 Hz, 1H, Ar-*H*), 4.15 (p, *J* = 6.8 Hz, 1H, ^{i}Pr-C*H*), 3.19 – 3.07 (m, 1H, ^{i}Pr-C*H*), 2.79 (qd, *J* = 6.7,

3.9 Hz, 2H, ^{i}Pr-C*H*), 2.64 (s, 3H, CH_3), 2.38 (d, *J* = 13.7 Hz, 1H, ring-CH_2), 2.16 (d, *J* = 13.6 Hz, 1H, ring-CH_2), 1.88 (d, *J* = 6.6 Hz, 3H, CH_3), 1.60 – 1.47 (m, 9H, CH_3), 1.45 – 1.36 (m, 9H, CH_3), 1.33 (d, *J* = 6.7 Hz, 3H, CH_3), 1.28 (s, 3H, CH_3), 0.58 (d, *J* = 6.8 Hz, 3H, CH_3). $^{13}C\{^1H\}$ NMR (101 MHz, CD_2Cl_2) δ 219.4, 182.9, 145.6, 144.5, 141.5, 138.7, 131.7, 130.8, 129.7, 128.9, 128.5, 127.8, 125.0, 124.6, 124.0, 123.5, 82.2, 78.1, 45.4, 31.4, 30.7, 29.8, 29.8, 29.5, 28.1, 27.5, 27.0, 25.1, 24.4, 24.4, 24.0, 23.8, 23.6, 21.6. Anal. Calc. for $C_{38}H_{50}Cl_2N_2Pd$: C, 64.09; H, 7.08; N, 3.93. Found: C 63.77; H, 7.11; N, 3.97.

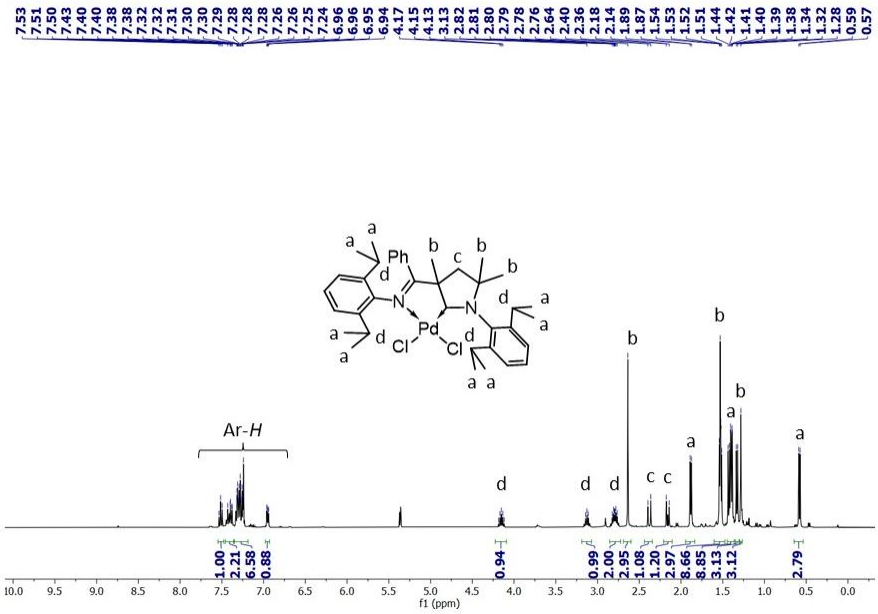

Figure-S51. ^{1}H NMR spectrum (400 MHz) of **E'** in CD_2Cl_2.

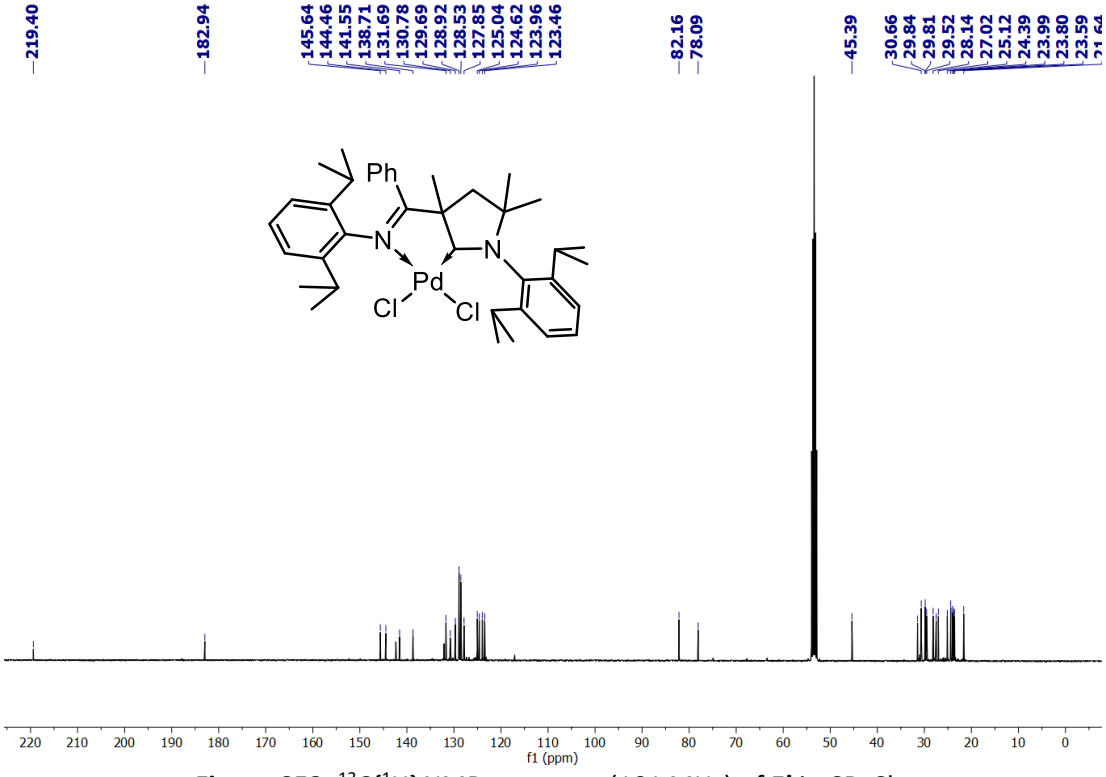

Figure-S52. $^{13}C\{^1H\}$ NMR spectrum (101 MHz) of **E'** in CD_2Cl_2.

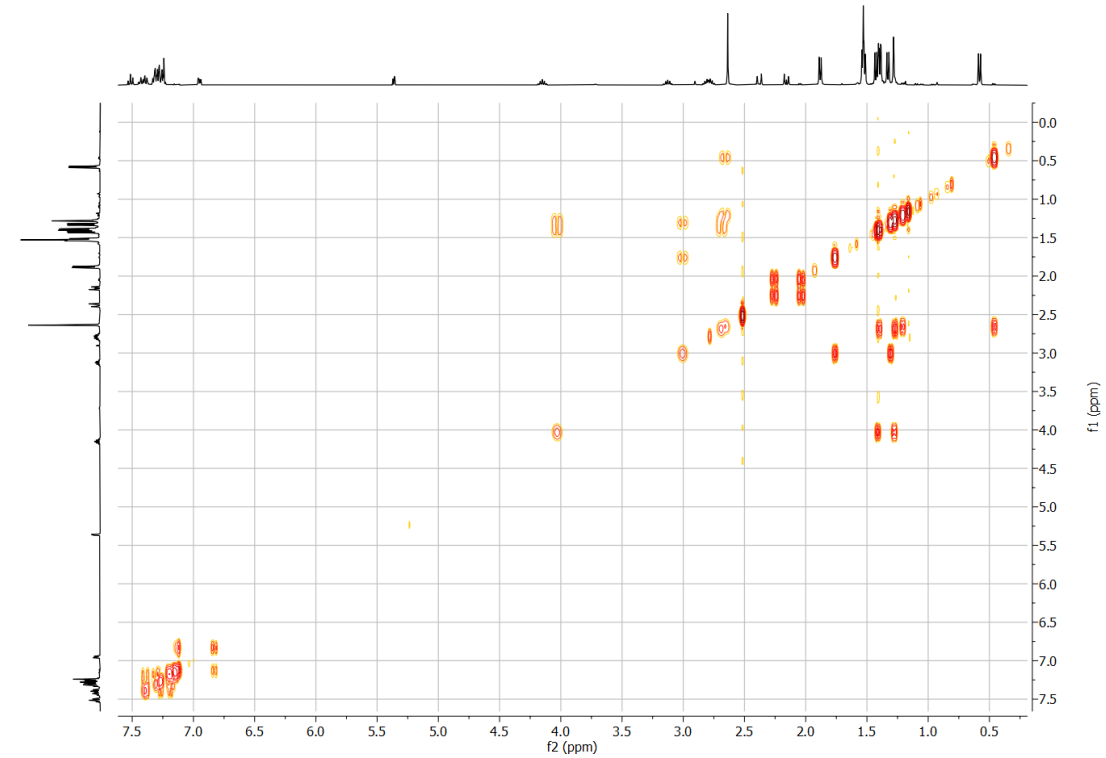

Figure S53. (^{1}H -^{1}H) COSY NMR spectrum (400 MHz) of **E'** in CD_2Cl_2.

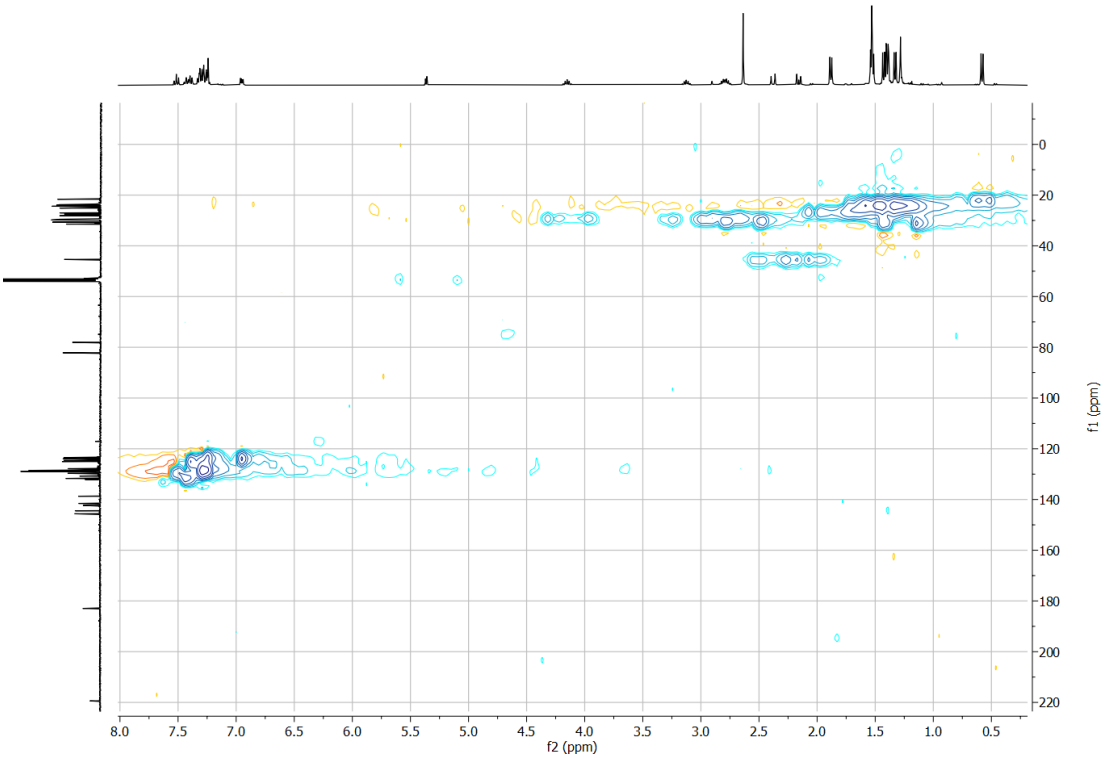

Figure S54. (^{1}H -^{13}C) HSQC NMR spectrum (400 MHz) of **E'** in CD_2Cl_2.

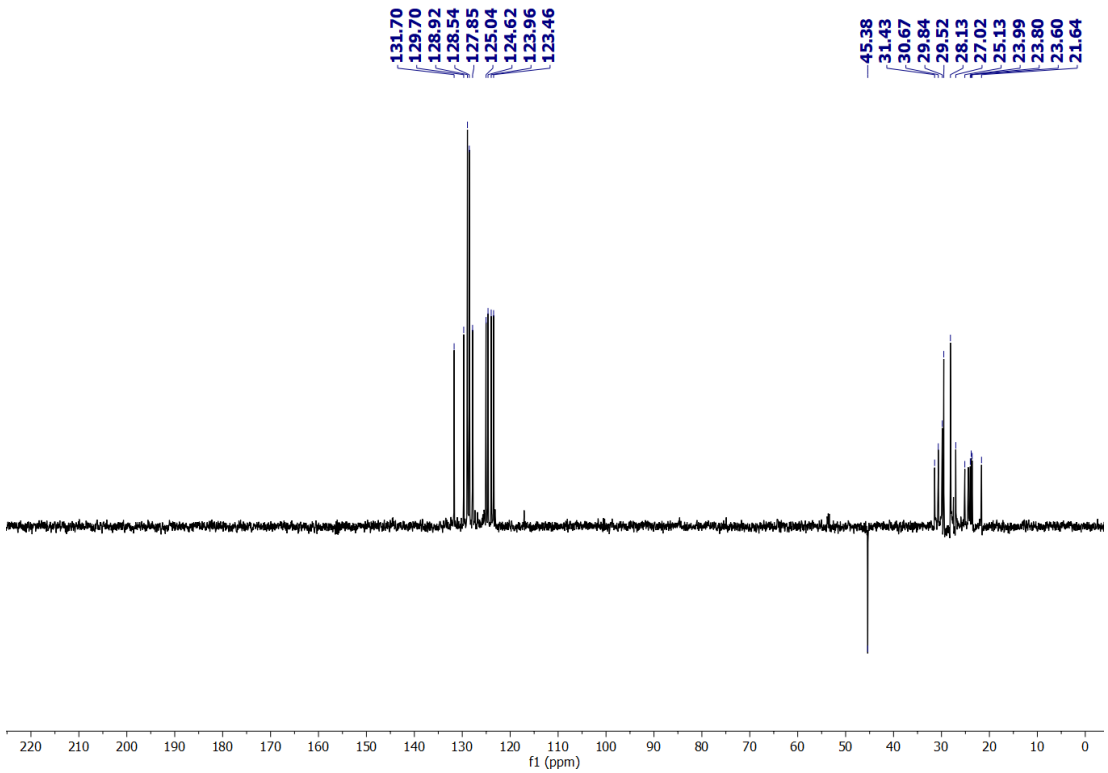

Figure S55. DEPT-^{13}C NMR spectrum (101 MHz) of **E'** in CD_2Cl_2.

Comparison of 4, 5, and E' for the coupling between *p*-Me-C_6H_4Cl and PhNHMe under identical conditions (0.5 mol% w.r.t. Pd; 100 °C).

A 25 mL Teflon-stoppered storage flask fitted with a magnetic bar was charged with *p*-Me-C_6H_4Cl (1.04 mmol), PhNHMe (1.14 mmol), NaO^{t}Bu (1.14 mmol), the precatalyst **4**/**5**/**E'** (5.2×10^{-3} mmol w.r.t. Pd, 0.5 mol%), 1,3,5-trimethoxybenzene (0.52 mmol, internal standard), and 2 mL of toluene. The mixture was then heated at 100 °C under constant stirring and the reaction progress was followed by taking aliquots time to time and monitoring the decrease in concentration of *p*-Me-C_6H_4Cl with respect to the internal standard through ^{1}H NMR spectroscopy.

TOF (at the 1 h mark) for **4**: 62 h^{-1}.

TOF (at the 1 h mark) for **E'**: 69 h^{-1}.

TOF (at the 1 h mark) for **5**: 88 h^{-1}.

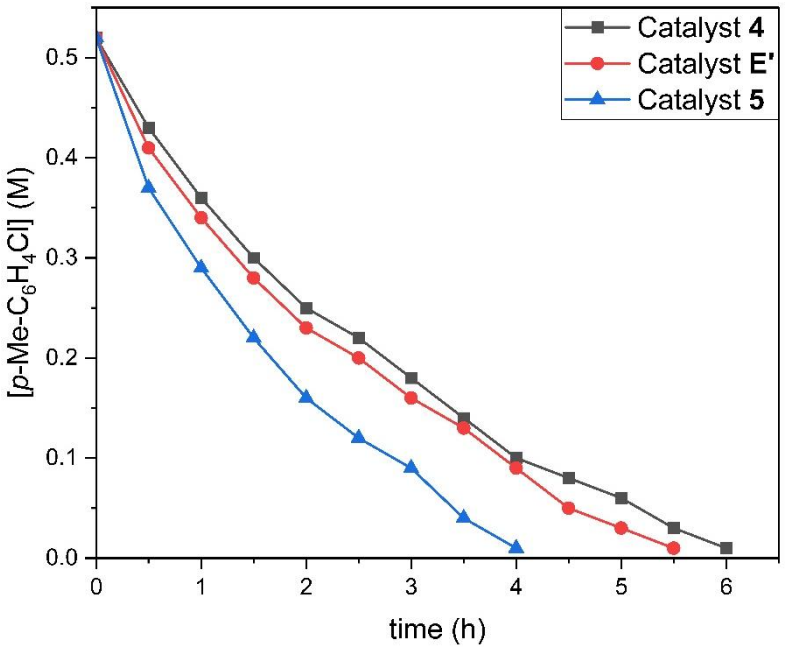

Figure S56. [*p*-Me-C_6H_4Cl] (M) vs. time (h) plot for the comparative catalysis of **4**, **E'**, and **5**.

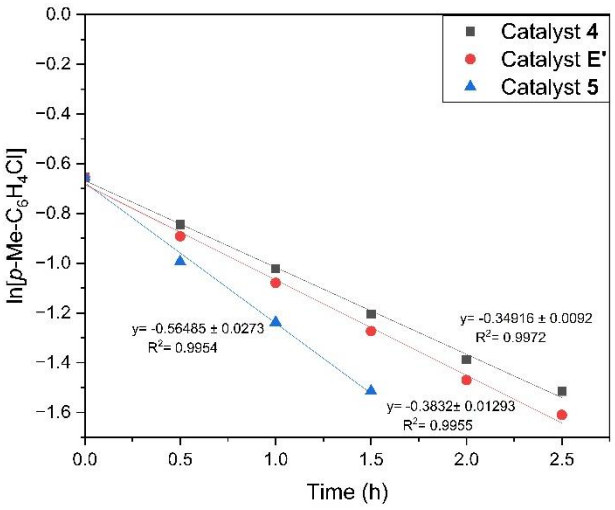

Figure S57. Plots of Ln[*p*-Me-C_6H_4Cl] vs. time (h) up to the 1st half-life for runs with **4**, **E'**, and **5**.

Control runs with 10, 50, and 100% of TBACl and $TBABF_4$ as additives were conducted for both **4** and **5** under identical conditions as without them (effective Pd: 0.5 mol%, 100 °C) and aliquots were taken at the same time interval for a rigorous comparison. In each case, the concentration profile vs. time remains the same as without the additives.

PXRD data of the grey precipitate collected after the catalysis:

The PXRD was performed using the Rigaku Miniflex 600 instrument integrated with a D/tex ultradetector to identify the phase of the as-prepared materials. The instrument consists of an X-ray target source CuK_α (λ = 1.54 Å), integrated with a 2.5° solar slit and a K_β filter. All the measurements were performed with an operating voltage of 40 kV and a tube current of 15 mA. The scan speed was maintained at 2°/min, and the range was maintained at 5−80°. The intensity vs 2θ plot was made using the Origin 2024 program.

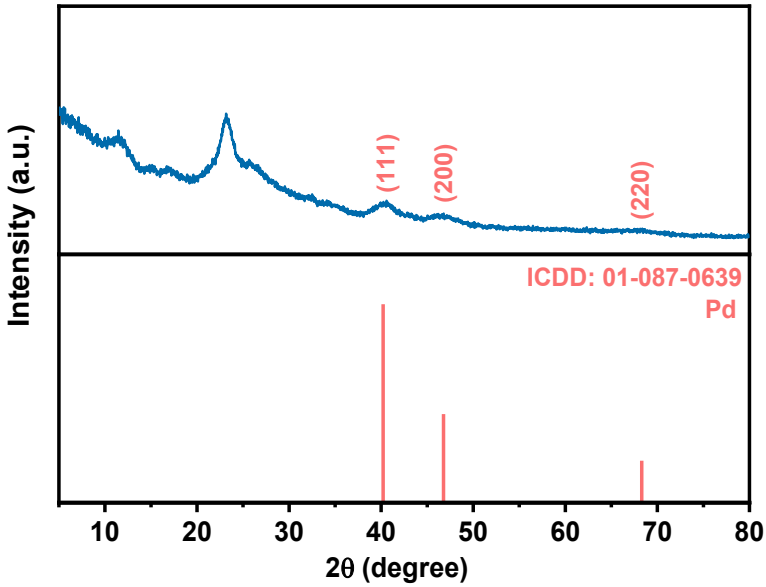

Figure S58. PXRD pattern of the grey precipitate collected.

3. Crystallographic Data.

X-ray diffraction data of complex **2**, **3**, **4**, and **5** were collected on a Rigaku XtaLAB Synergy i, Dualflex four-circle diffractometer with HyPix3000 detector using Cu-K_α radiation. Measurements were carried out at 100 K for all the compounds. The structures were solved by intrinsic phasing using SHELXT.[12] All refinements were carried out against F2 with ShelXL[13] as implemented in the program system Olex2.[14] The non-hydrogen atoms were refined with anisotropic displacement parameters. All hydrogen atoms were included in calculated positions and treated as riding throughout the refinement. **3** was refined as a two-component twin. Refinement results are given in Table

S3. Graphical representations were performed with the program DIAMOND.[15] CCDC- 2482323 (**2**), CCDC-2482324 (**3**), CCDC- 2482325 (**4**), and CCDC- 2482326 (**5**) contain the supplementary crystallographic data. These data can be obtained free of charge from the Crystallographic Data Centre via www.ccdc.cam.ac.uk/data_request/cif.

Table S2: Summary of crystallographic data for **2**-**5**.

	2	**3**	**4**	**5**
formula	$C_{27}H_{34}Cl_2Cu_2N_2O$	$C_{27}H_{34}AgClN_2O$	$C_{27}H_{34}Cl_2N_2OPd$	$C_{61}H_{79}Cl_4F_{12}N_7O_2Pd_2Sb_2$
Fw /g·mol^{-1}	600.54	545.88	579.86	1768.41
cryst. colour, habit	Colourless, Plate	Colourless, Plate	Light yellow, Block	Yellow, Block
crystal size/mm	0.26 × 0.25 × 0.07	0.234 × 0.152 × 0.067	0.21 × 0.14 × 0.11	0.33 × 0.16 × 0.16
crystal system	monoclinic	monoclinic	orthorhombic	orthorhombic
space group	*P2$_1$/c*	*P2$_1$/c*	*Pbca*	*Pbca*
a / Å	16.8500(2)	8.24670(10)	17.5214(2)	20.4946(2)
b / Å	14.97680(10)	17.11260(10)	16.08820(10)	25.3444(2)
c / Å	11.32490(10)	18.05060(10)	20.5334(2)	25.5099(2)
α / °	90	90	90	90
β / °	109.1820(10)	100.5240(10)	90	90
γ / °	90	90	90	90
V / Å^3	2699.27(5)	2504.50(4)	5788.12(9)	13250.4(2)
Z	4	4	8	8
d_{calc}/Mg·m^{-3}	1.478	1.448	1.331	1.773
μ(CuKα)/mm^{-1}	3.930	7.593	7.018	12.902 (CuKα)
F(000)	1240.0	1128.0	2384.0	7040.0
2θ range / °	5.554 to 136.306	7.176 to 136.446	8.612 to 136.416	6.54 to 136.804
index ranges	*-20 ≤ h ≤ 20, -18 ≤ k ≤ 16, -13 ≤ l ≤ 13*	*-9 ≤ h ≤ 9, -20 ≤ k ≤ 20, -20 ≤ l ≤ 21*	*-20 ≤ h ≤ 21, -19 ≤ k ≤ 19, -24 ≤ l ≤ 20*	*-24 ≤ h ≤ 24, -30 ≤ k ≤ 30, -29 ≤ l ≤ 30*
refln.	35231	30653	67947	160793
independ. reflns (R_{int})	4905 [R_{int} = 0.0547, R_{sigma} = 0.0246]	4551 [R_{int} = 0.0536, R_{sigma} = 0.0232]	5281 [R_{int} = 0.0566, R_{sigma} = 0.0195]	12065 [R_{int} = 0.0852, R_{sigma} = 0.0282]
observed reflns	4593	4208	5019	10970
data/ restr./ param.	4905/0/314	4551/0/383	5281/0/305	12065/0/717
R_1, wR_2 [$I > 2\sigma(I)$]	*R_1 = 0.0340, wR_2 = 0.0963*	*R_1 = 0.0419, wR_2 = 0.1112*	*R_1 = 0.0424, wR_2 = 0.1132*	*R_1 = 0.0686, wR_2 = 0.1619*

R_1, wR_2 (all data)	R_1 = 0.0354, wR_2 = 0.0978	R_1 = 0.0443, wR_2 = 0.1134	R_1 = 0.0443, wR_2 = 0.1149	R_1 = 0.0443, wR_2 = 0.1149
GooF on F^2	1.027	1.047	1.023	1.024
largest diff. peak, hole/ e·Å^3	0.75/-0.56	1.38/-0.89	1.73/-1.36	3.43/-4.24
CCDC number	**2482323**	**2482324**	**2482325**	**2482326**

4. **DFT Analyses.**

Density Functional Theory (DFT) studies were undertaken using ORCA 6.0.1 program.[16] The structures were optimized using the B3LYP[17] functional with Grimme's D3 parameter set with Becke-Johnson (BJ) damping (D3BJ) for the dispersion correction.[18] The auxiliary basis SARC/J, along with the Resolution of the Identity J-Integral, Chain-Of-Spheres Exchange (RIJCOSX) method,[19] was used to speed up the calculations. ZORA-def2-SVP basis set was used to describe all atoms except Pd, for which SARC-ZORA-TZVP was used.[20] All optimizations were carried out using the SMD solvation model[21] with parameters corresponding to toluene to mimic the experimental conditions. This combination is referred to as the B3LYP-D3BJ/BS1 level of theory. The stationary points were characterized by the vibrational frequency analysis. The energy values were refined by single-point energy calculations using B3LYP-D3BJ method (SARC/J auxiliary basis set with RIJCOSX) with the SARC-ZORA-TZVPP basis on Pd and ZORA-def2-TZVP on the rest of the atoms, and toluene as solvent (SMD model). This level of theory is referred to as the B3LYP-D3BJ/BS2 level of theory. The natural bond orbital (NBO)[22] and Quantum theory of atoms in molecules (QTAIM)[23] analyses were performed at B3LYP-D3BJ/def2-TZVP//B3LYP-D3BJ/BS1 level of theory. The Multiwfn[24] program was used to analyze the wavefunction files and print the bond critical points. Energy decomposition analyses were carried out with the Xiamen Valence Bond (XMVB)[25] quantum chemistry program at B3LYP-D3BJ/def2-TZVP//B3LYP-D3BJ/BS1 level of theory.

NBO analysis:

The NBO method can describe an N-electron wavefunction in terms of localized orbitals which corresponds to the Lewis concept of chemical bonding. It provides a localized picture of bonding and donor-acceptor interactions. The second-order Fock matrix analysis provides the stabilization energy E(2) associated with the delocalization (2e stabilization) $i \rightarrow j$ for each donor (i) and acceptor (j) and is estimated as:

$$\mathrm{E}(2) = \Delta E_{ij} = q_i \frac{F_{ij}^2}{\varepsilon_i - \varepsilon_j}$$

where q_i is the donor orbital occupancy, ε_i, ε_j are diagonal elements (orbital energies) and $F_{i,j}$ is the off-diagonal NBO Fock matrix element.

Table S3. Second-order perturbation theory analysis of Fock matrix in NBO basis.

	Donor NBO (i) / occupancy	**Acceptor NBO (j) / occupancy**	**E(2) in kcal/mol**
$TS_{Id\text{-}Ie}$	LP C_{CAAC} (41% s; 59% p) / 1.640	LP* Pd (90% s) / 0.349	120.15
$TS_{IId\text{-}IIe}$	LP C_{CAAC} (41% s; 59% p) / 1.635	LP* Pd (91% s) / 0.323	109.17
$TS_{IIId\text{-}IIIe}$	LP C_{CAAC} (40% s; 60% p) / 1.611	LP* Pd (91% s) / 0.400	136.37
$TS_{IVd\text{-}IVe}$	LP C_{CAAC} (40% s; 60% p) / 1.632	LP* Pd (95% s) / 0.298	95.63

QTAIM analysis:

Covalent and non-covalent interactions can be distinguished by the electron density(ρ) at the bond critical point (BCP). In case of covalent interactions, the value of ρ is large (>0.1) while its Laplacian $\nabla^2\rho$ at BCP is negative; non-covalent interactions have a small value of ρ with a positive value of $\nabla^2\rho$. Local electronic energy density, H_{BCP} can be used for further differentiation between covalent and non-covalent interactions along with the $\nabla^2\rho$ at BCP. Covalent interactions have $\nabla^2\rho < 0$ and $H_{BCP} < 0$, partially covalent interactions or strong electrostatic interactions have $\nabla^2\rho > 0$ and $H_{BCP} < 0$; whereas, weaker non-covalent interactions have $\nabla^2\rho > 0$ and $H_{BCP} > 0$.

Table S4. Selected topological parameters.

	BCP	ρ	$\nabla^2\rho$	H_{BCP} in a.u.
$\mathbf{I_b}$	C_{CAAC}–Pd	0.116	0.357	–0.040
	N_{imine}–Pd	0.027	0.082	–0.002
$\mathbf{II_b}$	C_{CAAC}–Pd	0.126	0.364	–0.049
$\mathbf{TS_{Ib\text{-}Ic}}$	C_{CAAC}–Pd	0.131	0.360	–0.052
	N_{imine}–Pd	0.022	0.063	–0.009
$\mathbf{TS_{IIb\text{-}IIc}}$	C_{CAAC}–Pd	0.125	0.340	–0.047
$\mathbf{I_e}$	C_{CAAC}–Pd	0.144	0.383	–0.064
	N_{imine}–Pd	0.021	0.061	–0.006
$\mathbf{II_e}$	C_{CAAC}–Pd	0.150	0.381	–0.069

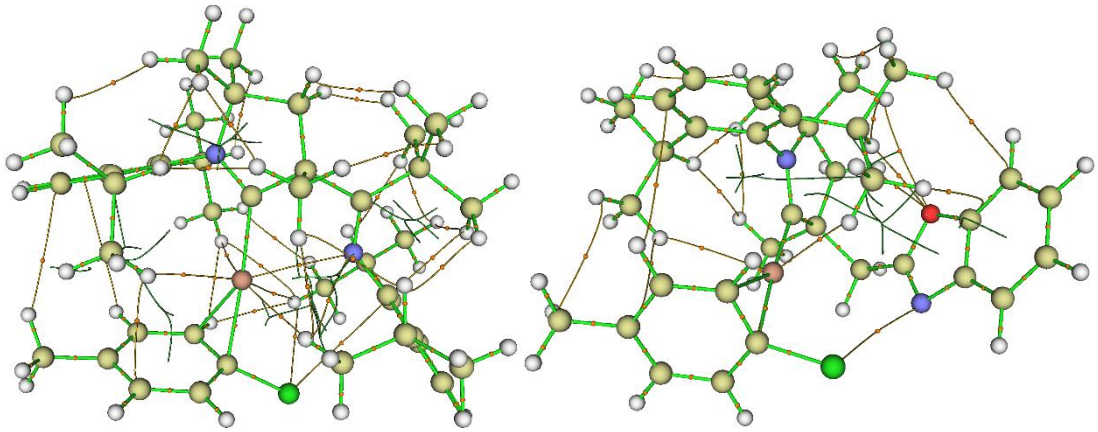

Figure S59. BCPs of $\mathbf{I_b}$ (left) **and** $\mathbf{II_b}$ (right).

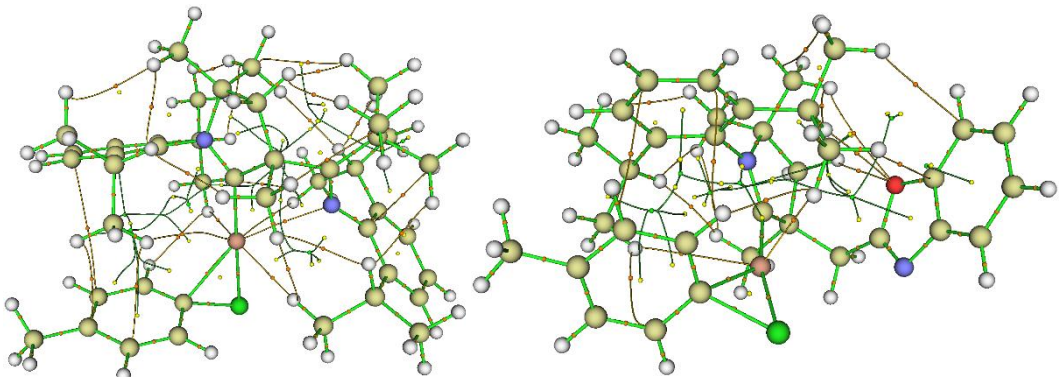

Figure S60. BCPs of $\mathbf{TS_{Ib\text{-}Ic}}$ (left) **and** $\mathbf{TS_{IIb\text{-}IIc}}$ (right).

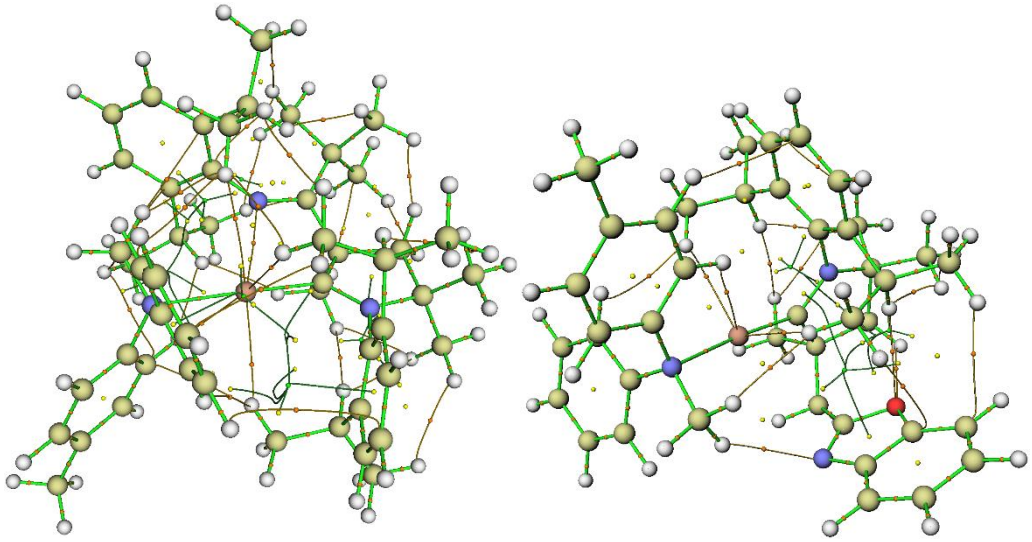

Figure S61. BCPs of $\mathbf{I_e}$ (left) **and** $\mathbf{II_e}$ (right).

Energy Decomposition Analysis:

The total interaction energy between two fragments is decomposed into electrostatic, exchange, repulsion, polarization, correlation and dispersion terms:

$$\Delta E_{int} = \Delta E_{els} + \Delta E_{exc} + \Delta E_{rep} + \Delta E_{pol} + \Delta E_{corr} + \Delta E_{disp}$$

The fragments considered are highlighted in different colours.

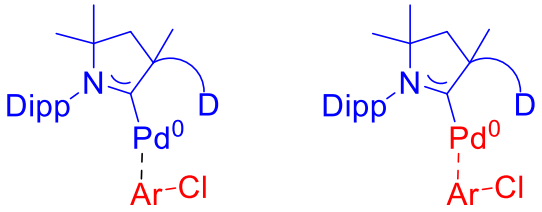

(i) (ii)

Table S5. EDA of **I_b** and **II_b**. Energy values given in kcal/mol.

	D	ΔE_{els}	ΔE_{exc}	ΔE_{rep}	ΔE_{pol}	ΔE_{corr}	ΔE_{disp}	ΔE_{int}
(i)	imine	–309.62	–356.93	780.84	–147.55	–42.28	–21.91	–97.46
	benzoxazole	–258.79	–296.50	643.78	–116.69	–42.10	–15.39	–85.70
(ii)	imine	–353.69	–312.17	717.44	–95.86	–64.49	–31.53	–140.31
	benzoxazole	–398.59	–341.40	805.50	–101.51	–58.30	–22.20	–116.50

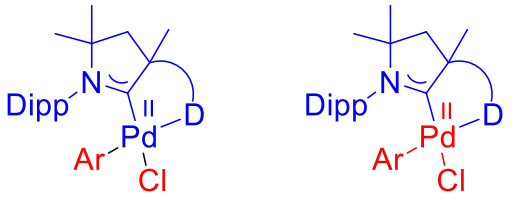

(iii) (iv)

Table S6. EDA of **I_c** and **II_c**. Energy values given in kcal/mol.

	D	ΔE_{els}	ΔE_{exc}	ΔE_{rep}	ΔE_{pol}	ΔE_{corr}	ΔE_{disp}	ΔE_{int}
(iii)	imine	–724.61	–422.96	973.74	–245.55	–38.47	–23.32	–481.17
	benzoxazole	–742.20	–396.72	949.70	–233.15	–40.39	–19.95	–482.71
(iv)	imine	–405.19	–330.29	819.50	–114.45	–61.75	–27.06	–119.24
	benzoxazole	–398.59	–341.40	805.50	–101.51	–58.30	–22.20	–116.50

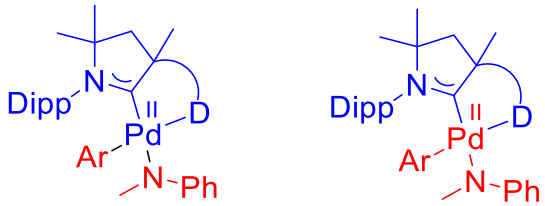

(v) (vi)

Table S7. EDA of **I_d** and **II_d**. Energy values given in kcal/mol.

	D	ΔE_{els}	ΔE_{exc}	ΔE_{rep}	ΔE_{pol}	ΔE_{corr}	ΔE_{disp}	ΔE_{int}
(v)	imine	–761.19	–467.44	1079.34	–266.06	–41.04	–31.81	–488.21
	benzoxazole	–767.71	–413.73	1011.44	–253.36	–46.72	–29.63	–499.72
(vi)	imine	–402.33	–339.73	823.31	–111.83	–63.30	–37.23	–131.11
	benzoxazole	–396.13	–333.92	814.03	–105.50	–66.53	–33.52	–121.56

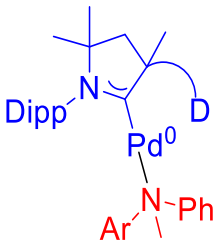

Table S8. EDA of $\mathbf{I_e}$ and $\mathbf{II_e}$. Energy values given in kcal/mol.

D	ΔE_{els}	ΔE_{exc}	ΔE_{rep}	ΔE_{pol}	ΔE_{corr}	ΔE_{disp}	ΔE_{int}
imine	–178.63	–230.82	459.93	–61.06	–31.46	–27.19	–69.23
benzoxazole	–184.68	–224.99	458.54	–65.66	–29.58	–19.45	–65.82

The above energy decomposition analysis shows L^1 to consistently have a stronger interaction than L^2, even when the relative stability order is flipped at the **Id**/**IId** stage.

Table S9. Electronic energy (E), Zero-Point energy (ZPE) and Thermal correction to Gibbs free energy (G_{corr}) values given in Hartree (E_h) and imaginary frequencies of optimized structures calculated at 298.15 K and 1 atm pressure.

	Imaginary frequency (cm^{-1})	E at B3LYP-D3BJ/BS1 level	ZPE at B3LYP-D3BJ/BS1 level	G_{corr} at B3LYP-D3BJ/BS1 level	E at B3LYP-D3BJ/BS2 level
Ia	-	–6888.369108	0.954310	0.881122	–6890.211322
Ib	-	–7350.039782	0.944453	0.870275	–7352.041851
TS_{Ib-Ic}	–187.13	–7350.018645	0.943663	0.868830	–7352.022552
Ic	-	–7350.100127	0.948144	0.875238	–7352.101412
Ic-cis	-	–7350.081810	0.947467	0.873770	–7352.082793
Id	-	–7213.919863	1.082435	1.003271	–7216.106111
Id-cis	-	–7213.907580	1.081956	1.004537	–7216.093546
TS_{Id-Ie}	–387.63	–7213.877538	1.080342	1.001219	–7216.061593
Ie	-	–7213.923177	1.082106	1.002288	–7216.107043
IIa	-	–6608.802900	0.684866	0.621689	–6610.381671
IIb	-	–7070.469473	0.675044	0.611612	–7072.209529
$TS_{IIb-IIc}$	–217.78	–7070.449609	0.675938	0.611638	–7072.189796
IIc	-	–7070.525743	0.677771	0.615797	–7072.264098
IIc-cis	-	–7070.50928	0.676938	0.612876	–7072.247034
IId	-	–6934.359258	0.811537	0.743299	–6936.281717
IId-cis	-	–6934.347660	0.810429	0.741666	–6936.270111
$TS_{IId-IIe}$	–370.31	–6934.308702	0.809193	0.739535	–6936.229169
IIe	-	–6934.362120	0.814338	0.744917	–6936.282209

IIId	-	–6614.530974	0.779776	0.713621	–6616.099864
$TS_{IIId\text{-}IIIe}$	–371.74	–6614.501504	0.778377	0.712815	–6616.068632
IIIe	-	–6614.549172	0.780409	0.713760	–6616.114700
IVd	-	–6862.722208	0.870893	0.798730	–6864.554409
$TS_{IVd\text{-}IVe}$	–370.54	–6862.677414	0.869319	0.797538	–6864.507583
IVe	-	–6862.721191	0.871283	0.798030	–6864.553806
Toluene	-	–271.413465	0.127757	0.098798	–271.700268
ArCl	-	–733.079833	0.118313	0.085905	–733.529431
KOtBu	-	–836.455106	0.123130	0.090673	–836.797322
HNMePh	-	–326.746143	0.145143	0.113774	–327.0943182
KCl	-	–1065.797455	0.000594	-0.022846	–1066.054369
HOtBu	-	–233.578772	0.135460	0.106497	–233.836619

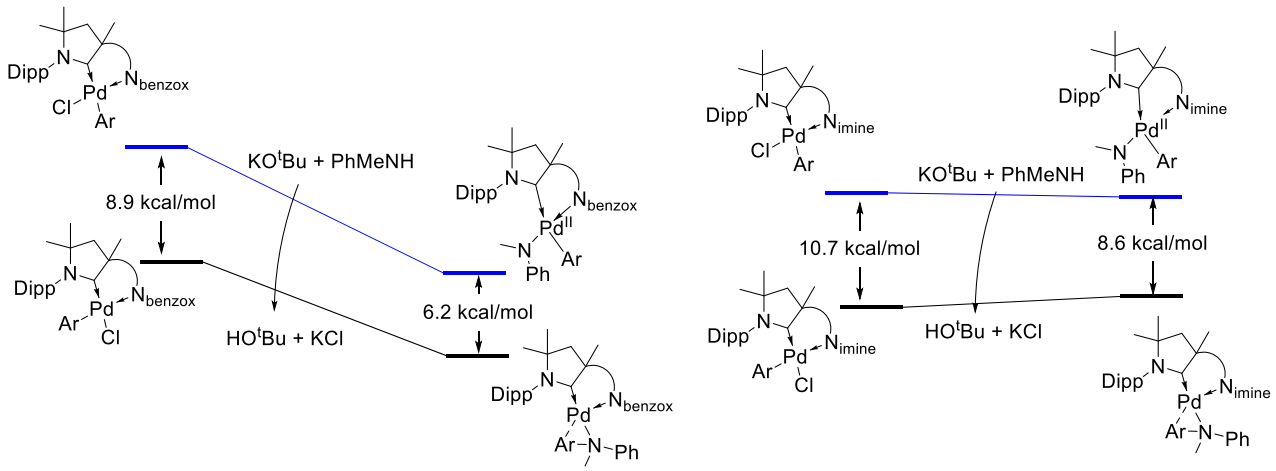

Figure S62. Comparison between Gibbs free energies for cis- and trans- isomers of **Ic**/**IIc** (***left***) and **Id**/**IId** (***right***).

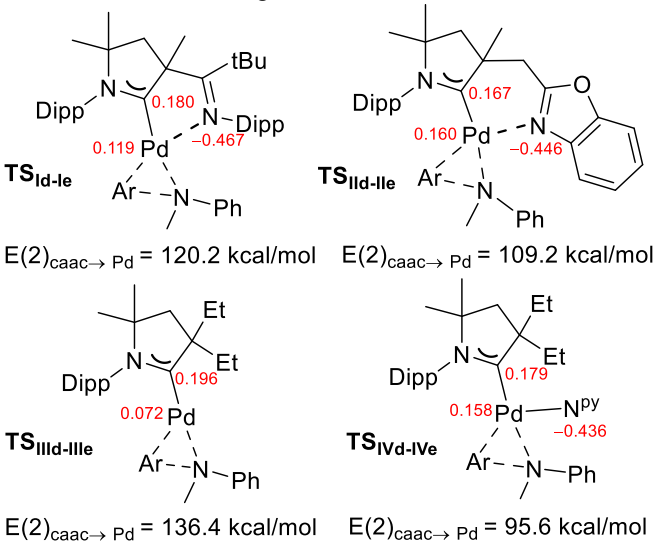

Figure S63. Natural charges (***in red***) and the stabilization energy E(2) from the interaction of the CAAC lone pair with Pd calculated using NBO method.

$E(2)_{CAAC \rightarrow Pd}$ stabilization energy is higher for L^1 in $\mathbf{TS_{Id\text{-}Ie}}$ (120.2 kcal/mol) than for L^2 in $\mathbf{TS_{IId\text{-}IIe}}$ (109.2 kcal/mol). The Pd in $\mathbf{TS_{Id\text{-}Ie}}$ also has a lower natural charge (0.119) than in $\mathbf{TS_{IId\text{-}IIe}}$ (0.160). Thus, L^1 renders a higher Pd^0 character than does L^2 in the *RE* transition state to justify its more facile nature. The $E(2)_{CAAC \rightarrow Pd}$ and natural charges for $\mathbf{TS_{IIId\text{-}IIIe}}$ and $\mathbf{TS_{IVd\text{-}IVe}}$ (Fig. 4) also suggest that the $Pd^{II} \rightarrow Pd^0$ reduction is most facile with ^{Et2}CAAC.

5. References.

1. S. Baguli, A. Kundu, S. Nath, D. Adhikari and D. Mukherjee, A Donor–Acceptor Cyclopropane by Intramolecular C(sp3)–H Activation at a Cyclic(alkyl)(amino)carbene Center and Its Fascinating Ring-Opening Chemistry, *Org. Lett.*, 2023, **25**, 3141-3145.
2. F. You, J. Wang, H. Liu, X. Kang and X. Shi, Phosphine-functionalized amidinate ligated rare-earth metal complexes for highly 3,4-selective living polymerization of 1,3-conjugated dienes, *Dalton Trans.*, 2023, **52**, 10760-10768.
3. J. Chu, D. Munz, R. Jazzar, M. Melaimi and G. Bertrand, Synthesis of Hemilabile Cyclic (Alkyl)(amino)carbenes (CAACs) and Applications in Organometallic Chemistry, *J. Am. Chem. Soc.*, 2016, **138**, 7884-7887.
4. N. Marigo, B. Morgenstern, A. Biffis and D. Munz, (CAAC)Pd(py) Catalysts Disproportionate to Pd(CAAC)2, *Organometallics*, 2023, **42**, 1567-1572.
5. S. Ostrowska, A. Czapik, M. Kwit and S. P. Nolan, Palladates of the [NHC·H][Pd(NH2)(CC)Cl2] Type as Effective Pre-catalysts for the Formation of C−C and C−N Bonds, *ChemCatChem*, 2023, **15**, e202301124.
6. A. de Gombert, A. Darù, T. S. Ahmed, M. C. Haibach, R. Li-Matsuura, C. Yang, R. F. Henry, S. P. Cook, S. Shekhar and D. G. Blackmond, Mechanistic Insight into Cu-Catalyzed C–N Coupling of Hindered Aryl Iodides and Anilines Using a Pyrrol-ol Ligand Enables Development of Mild and Homogeneous Reaction Conditions, *ACS Catal.*, 2023, **13**, 2904-2915.
7. S. G. Rull, I. Funes-Ardoiz, C. Maya, F. Maseras, M. R. Fructos, T. R. Belderrain and M. C. Nicasio, Elucidating the Mechanism of Aryl Aminations Mediated by NHC-Supported Nickel Complexes: Evidence for a Nonradical Ni(0)/Ni(II) Pathway, *ACS Catal.*, 2018, **8**, 3733-3742.
8. S. Nagumo, Y. Ishii, G. Sato, M. Mizukami, M. Imai, N. Kawahara and H. Akita, 8-Endo selective Friedel–Crafts cyclization of vinyloxiranes with Co2(CO)6-complexed acetylene, *Tetrahedron Lett.*, 2009, **50**, 26-28.
9. A. M. Fiore, R. Ciciriello, D. Blasi, P. Cotugno, A. Punzi and G. M. Farinola, Infrared Irradiation-Assisted Green Approach for Pd-Catalyzed Buchwald–Hartwig Amination, *Chem. Eur. J.*, 2025, **31**, e202500557.
10. M. Rodriguez Moreno, M. L. Setelin, J. D. Hansen, J. L. Corey, K. L. Noble, L. R. Stillwell, E. Angell, O. A. Stubbs, J. Kumawat, C. S. Muñoz Gomez, S. J. Smith, D. H. Ess and D. J. Michaelis, Controlling Catalyst Speciation to Achieve Room Temperature Pd-Catalyzed Aminations with Aryl and Heteroaryl Chlorides, *Adv. Synth. Catal.*, 2025, **367**, e202401337.
11. S. Kräh, I. Kachel and O. Trapp, Electron-Rich Silicon Containing Phosphinanes for Rapid Pd-Catalyzed C−X Coupling Reactions, *ChemCatChem*, 2022, **14**, e202200734.
12. G. Sheldrick, SHELXT - Integrated space-group and crystal-structure determination, *Acta Crystallogr., Sect. A: Found. Adv.*, 2015, **71**, 3-8.
13. G. Sheldrick, Crystal structure refinement with SHELXL, *Acta Crystallogr., Sect. C: Struct. Chem.*, 2015, **71**, 3-8.
14. O. V. Dolomanov, L. J. Bourhis, R. J. Gildea, J. A. K. Howard and H. Puschmann, OLEX2: a complete structure solution, refinement and analysis program, *J. Appl. Crystallogr.*, 2009, **42**, 339-341.
15. K. Brandenburg and H. Putz, Diamond version 3, *Crystal Impact GbR, Bonn, Germany*, 2005.
16. F. Neese, The ORCA program system, *Wiley Interdiscip. Rev.:Comput. Mol. Sci.*, 2012, **2**, 73-78.
17. (a) C. Lee, W. Yang and R. G. Parr, Development of the Colle-Salvetti correlation-energy formula into a functional of the electron density, *Phys. Rev. B*, 1988, **37**, 785-789; (b) A. D. Becke,

Density-functional thermochemistry. III. The role of exact exchange, *J. Chem. Phys.*, 1993, **98**, 5648-5652.
18. H. Schröder, A. Creon and T. Schwabe, Reformulation of the D3(Becke–Johnson) Dispersion Correction without Resorting to Higher than C6 Dispersion Coefficients, *J. Chem. Theory Comput.*, 2015, **11**, 3163-3170.
19. S. Kossmann and F. Neese, Efficient Structure Optimization with Second-Order Many-Body Perturbation Theory: The RIJCOSX-MP2 Method, *J. Chem. Theory Comput.*, 2010, **6**, 2325-2338.
20. F. Weigend and R. Ahlrichs, Balanced basis sets of split valence, triple zeta valence and quadruple zeta valence quality for H to Rn: Design and assessment of accuracy, *Phys. Chem. Chem. Phys.*, 2005, **7**, 3297-3305.
21. A. V. Marenich, C. J. Cramer and D. G. Truhlar, Universal Solvation Model Based on Solute Electron Density and on a Continuum Model of the Solvent Defined by the Bulk Dielectric Constant and Atomic Surface Tensions, *J. Phys. Chem. B*, 2009, **113**, 6378-6396.
22. E. D. Glendening, C. R. Landis and F. Weinhold, Natural bond orbital methods, *Wiley Interdiscip. Rev.: Comput. Mol. Sci.*, 2011, **2**, 1-42.
23. F. Cortés-Guzmán and R. F. W. Bader, Complementarity of QTAIM and MO theory in the study of bonding in donor–acceptor complexes, *Coord. Chem. Rev.*, 2005, **249**, 633-662.
24. T. Lu and F. Chen, Multiwfn: A multifunctional wavefunction analyzer, *J. Comput. Chem.*, 2012, **33**, 580-592.
25. (a) L. Song, W. Wu, Q. Zhang and S. Shaik, A practical valence bond method: A configuration interaction method approach with perturbation theoretic facility, *J. Comput. Chem.*, 2004, **25**, 472-478; (b) Z. Chen and W. Wu, Ab initio valence bond theory: A brief history, recent developments, and near future, *J. Chem. Phys.*, 2020, **153**, 090902.